Available online at www.sciencedirect.com

ScienceDirect

Journal of Nutritional Biochemistry 116 (2023) 109322

Journal of Nutritional Biochemistry

RESEARCH PAPER

Vitamin D receptor regulates transcription of mitochondrial DNA and directly interacts with mitochondrial DNA and TFAM

Duygu Gezen-Ak[a], Merve Alaylıoğlu[a], Zuhal Yurttaş[a], Tugay Çamoğlu[a], Büşra Şengül[b], Cihan İşler[c], Ümit Yaşar Kına[d], Ebru Keskin[b], İrem Lütfiye Atasoy[b], Ali Metin Kafardar[c], Mustafa Uzan[c], Cedric Annweiler[e,f,g], Erdinç Dursun[a,*]

[a] Brain and Neurodegenerative Disorders Research Laboratories, Department of Neuroscience, Institute of Neurological Sciences, Istanbul University-Cerrahpasa, Istanbul, Turkey
[b] Department of Medical Biology, Cerrahpasa Faculty of Medicine, Istanbul University-Cerrahpasa, Istanbul, Turkey
[c] Department of Neurosurgery, Cerrahpasa Faculty of Medicine, Istanbul University-Cerrahpasa, Istanbul, Turkey
[d] Beykoz Institute of Life Sciences and Biotechnology, Bezmialem Vakif University, Istanbul, Turkey
[e] Department of Geriatric Medicine and Memory Clinic, Research Center on Autonomy and Longevity, University Hospital, Angers, France
[f] UPRES EA 4638, University of Angers, Angers, France
[g] Robarts Research Institute, Department of Medical Biophysics, Schulich School of Medicine and Dentistry, The University of Western Ontario, London, Ontario, Canada

Received 11 October 2022; received in revised form 15 March 2023; accepted 15 March 2023

Abstract

Vitamin D receptor (VDR) is an essential transcription factor (TF) synthesized in different cell types. We hypothesized that VDR might also act as a mitochondrial TF. We conducted the experiments in primary cortical neurons, PC12, HEK293T, SH-SY5Y cell lines, human peripheral blood mononuclear cells (PBMC) and human brain. We showed that vitamin D/VDR affects the expression of mitochondrial DNA (mtDNA) encoded oxidative phosphorylation (OXPHOS) subunits. We observed the co-localization of VDR with mitochondria and the mtDNA with confocal microscopy. mtDNA-chromatin-immunoprecipitation and electrophoretic mobility shift assays indicated that VDR was able to bind to the mtDNA D-loop site in several locations, with a consensus sequence "**MMHKCA**." We also reported the possible interaction between VDR and mitochondrial transcription factor A (TFAM) and their binding sites located in close proximity in mtDNA. Consequently, our results showed for the first time that VDR was able to bind and regulate mtDNA transcription and interact with TFAM even in the human brain. These results not only revealed a novel function of VDR, but also showed that VDR is indispensable for energy demanded cells.

Keywords: Vitamin D; Vitamin D receptor; Transcription factor; Mitochondrial transcription factor; Mitochondrial DNA; Mitochondria.

1. Introduction

Vitamin D3 (cholecalciferol) is taken in the diet or is synthesized from 7-dehydrocholesterol upon exposure to ultraviolet light B. Vitamin D is hydroxylated at C-25 in the liver by vitamin D 25-hydroxylase CYP27A1 (formation of 25-hydroxyvitamin D3), Then it is hydroxylated at the position of carbon 1 of the A ring in the proximal renal tubule by 1α-hydroxylase CYP27B1, resulting in the formation of 1-25-dihydroxyvitamin D3 or 1-25-dihydroxycholecalciferol (1α,25$(OH)_2D_3$), a hormonally active form of vitamin D [1]. In addition, an additional cytochrome P450 enzyme-CYP11A1 has been reported that has the ability to 20-hydroxylates vitamin D resulting formation of 20,23(OH)2D, which could act similarly to 1,25(OH)2D in different tissues [2–5].

The active form of vitamin D shows its effects with the nuclear hormone receptor, vitamin D receptor (VDR) [6,7]. VDR is one of the 1,900 transcription factors (TF) encoded in the human genome and is synthesized in many human tissues and different cell types. Results from VDR ChIP-seq data sets and ENCODE have shown that there may be 1,000–10,000 genomic VDR binding sites per cell type, and VDR combines with different coactivators and corepressors in the presence and absence of ligand [8]. Our previous studies showed that vitamin D3 and VDR have essential roles in the gene expression profile of neurons and neurodegeneration [9–28].

Mitochondria play a crucial role in the function and survival of neurons in the brain, one of the most energy-consuming organs of the human body. Long-lived, energy-dependent neurons provide very limited glycolysis while primarily providing their energy

* Corresponding author at: Erdinç Dursun, Department of Neuroscience, Institute of Neurological Sciences, 34098 Istanbul, Turkey. Tel.: +90 212 414 30 00/22032, +90 533 339 98 82.
E-mail address: erdinc.dursun@iuc.edu.tr (E. Dursun).

https://doi.org/10.1016/j.jnutbio.2023.109322
0955-2863/

from the mitochondrial oxidative phosphorylation (OXPHOS) system [29]. Functional disorders in mitochondria can increase oxidative stress and cause aging and neurodegeneration. Confirming this, mitochondrial dysfunction, mtDNA alterations, and oxidative stress are considered the most prominent features of age-related neurodegenerative diseases [29,30]. Additionally, recently we showed that systemic dysregulation of transcription of mitochondrial DNA (mtDNA) or mitochondrial quality control genes might result in the development of neurodegenerative disorders [22].

Today, we know that some steroid hormone receptors are also located in mitochondria. These receptors in mitochondria are believed to be the same or very similar to nuclear ones [31]. Glucocorticoid receptor (GR) or estrogen receptor (ER) is not only found in mitochondria but also interacts with mitochondrial DNA (mtDNA) [32,33]. Information on the relationship between VDR and mitochondria is a relatively new field.

In 2010, Silvagno et al. reported for the first time, the presence of VDR in the mitochondria of human platelets and differentiated megakaryocytes [34]. The same group found that VDR was translocated to mitochondria in the human keratinocyte cell line [35]. After silencing VDR in different cell types, including normal or cancer cell lines, researchers observed that the VDR protected cells from excessive respiration and ROS production. The absence of the receptor was suggested to cause impairment of mitochondrial integrity and cell death [36]. Ryan et al. showed that the mitochondrial oxygen consumption rate increased in $1\alpha,25(OH)_2D_3$-treated cells, and they suggested that 83 nuclear mRNAs encoding mitochondrial proteins were changed following $1\alpha,25(OH)_2D_3$ treatment of human skeletal muscle cells [37]. Dzik and Kaczor reviewed the effect of vitamin D on skeletal muscle function. They proposed that vitamin D deficiency, in the long run, induces VDR ablation, ROS generation, and consequent deleterious effects on mitochondrial function, leading to elevated muscle atrophy [38]. Lee et al. reported that $1\alpha,25(OH)_2D_3$ treatment increased 17β-estradiol secretion, the expression of mitochondrial biogenesis-related proteins, ATP production, and cellular oxygen consumption in primary rat granulosa cells [39]. Recently, Mocayar Marón et al. suggested that vitamin D and melatonin might synergistically protect proper mitochondrial functioning [40].

All these data might suggest another basic knowledge. As we know, VDR is a TF. However, TFAM regulates mtDNA transcription. Today we know that there are some other TFs in addition to TFAM for regulating the transcription of mtDNA [41–45]. Besides, some nuclear TFs can also migrate to mitochondria to directly regulate mitochondrial gene expression [33,46-48]. Additionally, Consiglio et al. conducted *in silico* analysis for screening mtDNA to identify vitamin D responsive element (VDRE) sites. They found two VDRE sites located in the displacement loop (D-loop), which have high-affinity cut-offs [49]. We hypothesized that VDR might serve as a TF for mtDNA. Given mitochondria have a central role in neuronal survival and neurodegeneration, and most of our studies focused on neurodegeneration and VDR, we conducted the present study with a perspective of the role of mitochondrial VDR action in neurodegeneration in primary cortical neurons.

First of all, we aimed to see the effect of vitamin D3 administration on the expression of mtDNA encoding oxidative phosphorylation (OXPHOS) subunits in primary cortical neurons. After that, we silenced or overexpressed VDR in neurons. For overexpression, we used an additional cell type, PC12, to understand if the answer would change according to the cell type. Our results led us to go one step further, and we showed mtDNA and VDR co-localization by confocal microscopy in primary cortical neurons and SH-SY5Y cells. To confirm this finding, we conducted mtDNA chromatin Immunoprecipitation (ChIP) assay in primary cortical neurons, HEK293T, SH-SY5Y cells, human peripheral blood mononuclear cells (PBMC) and human brain tissue showed that VDR was able to bind to mtDNA D-loop site. Furthermore, we determined possible binding sequences for VDR in the proximity of the TFAM binding site in the mtDNA D-loop region with electrophoretic mobility shift assay (EMSA). We also reported the possible interaction of VDR and TFAM by co-immunoprecipitation (IP) in HEK293T cells and human brain tissue.

2. Materials and methods

All methods performed in this study were summarized in Figure 1.

2.1. Samples

We aim to investigate whether VDR regulates mRNA expression of mtDNA encoded genes in most energy-depending cells like neurons. For this reason, rat primary neuron culture, the most preferred in neuroscience studies and obtained directly from the organism, was used as the main cell type. In addition, PC12 cells from the same species but with low VDR expression levels were used to show whether VDR affects the expression of genes encoded by mtDNA.

After determining the effect of vitamin D, VDR silencing or VDR overexpression on genes encoded by mtDNA, the answer to the question of whether VDR causes this effect by binding to mtDNA was investigated with different methods and different cells according to technical requirements and determining species and cell type differences:

- VDR co-localization with mtDNA was demonstrated by BrdU assay in rat primary cortical neurons and human SH-SY5Y cells.
- VDR binding to mtDNA was demonstrated by mtDNA-ChIP assay in primary cortical neurons, human cell lines (SH-SY5Y and HEK293T), and different human tissues (blood tissue-PBMCs and human brain tissue).
- A cell-free assay EMSA was used to determine the VDR interacting mtDNA sequences (HEK293T cell lysates were used for the VDR protein source).
- Co-IP was also performed to see if VDR, which binds to mtDNA and changes gene expression, has a relationship with TFAM. A human cell line (HEK293T) was used due to the high number of cell requirements, and human brain tissue was used to demonstrate the accuracy of the finding.

2.1.1. Primary cortical neuron culture

The neocortex of Sprague-Dawley rat embryos on embryonic d 16 (E16) was used to prepare primary neuron cultures as previously described [15,18]. Cells were incubated at 37°C in a 5% CO_2 humidified incubator for 7 d until neurons became mature. On culture d 7, 1,25 dihydroxyvitamin D3 treatments or silencing or overexpression of the VDR gene were performed to detect the effects of vitamin D3 and/or VDR on the expression of mitochondrial genes. Moreover, immunofluorescent labeling with neuronal (Millipore, MAB2300) and glial (Invitrogen, AB5804) markers was done to determine the neuron/glia ratio of the culture, as previously described [15,18]. VDR silencing or overexpression confirmed with VDR (Abcam, ab3508) immunofluorescent labeling. The Animal Welfare and Ethics Committee of Istanbul University approved the study with the number 26.07.2012/101. All procedures were conducted following the Istanbul University and National Research Council's guide for the care and use of laboratory animals [50].

2.1.2. HEK 293-T culture

HEK 293-T cells (ATCC, CRL-3216) were seeded at a density of 1×10^4 cell/cm^2 to 100 mm^2 petri dishes in DMEM (Gibco, 41966-029) supplemented with 10% fetal bovine serum (Gibco 10270-098) and incubated at 37°C and 5% CO_2 in a humidified incubator. The medium was changed every 2–3 d until the cells reached 80–90% confluency, and then the cells were subcultured. Subculturing included washing with 1X HBSS (Gibco, 14170-088), detachment with 0.05% trypsin-EDTA (Gibco, 25200-056), and centrifugation $125 \times g$ for 5–7 min at room temperature. After removing the supernatant, the cells were resuspended in fresh medium, seeded to 100 mm^2 petri dishes, and incubated at 37°C and 5% CO_2 atmosphere. HEK 293-T cells were used since they are accepted as a neuronal cell line, given they express most of the neuronal proteins [51].

2.1.3. PC12 cell culture and neuronal differentiation

PC12 cells (ATCC, CRL-1721) were cultured in a complete medium consisting of RPMI-1640 (Gibco, 302001) supplemented with 10% horse serum (Gibco, 16050-122), 5% fetal bovine serum (Gibco, 10270-098) and 50 units/mL antibiotic-antimycotic (Gibco, 15240-062), and incubated at 37°C and 5% CO_2 in a humidified atmosphere. The medium was replenished every 2–3 d. Cells were subcultured when they reached 80–90% confluency and then were seeded to 6-well plates at a density of 3×10^4 cells/cm^2 for neuronal differentiation. Differentiation was done via DMEM (Gibco, 41966-029) supplemented with 1% horse serum, 50 units/mL antibiotic-antimycotic, and 50 ng/mL nerve growth factor (Sigma, N6009). One-third

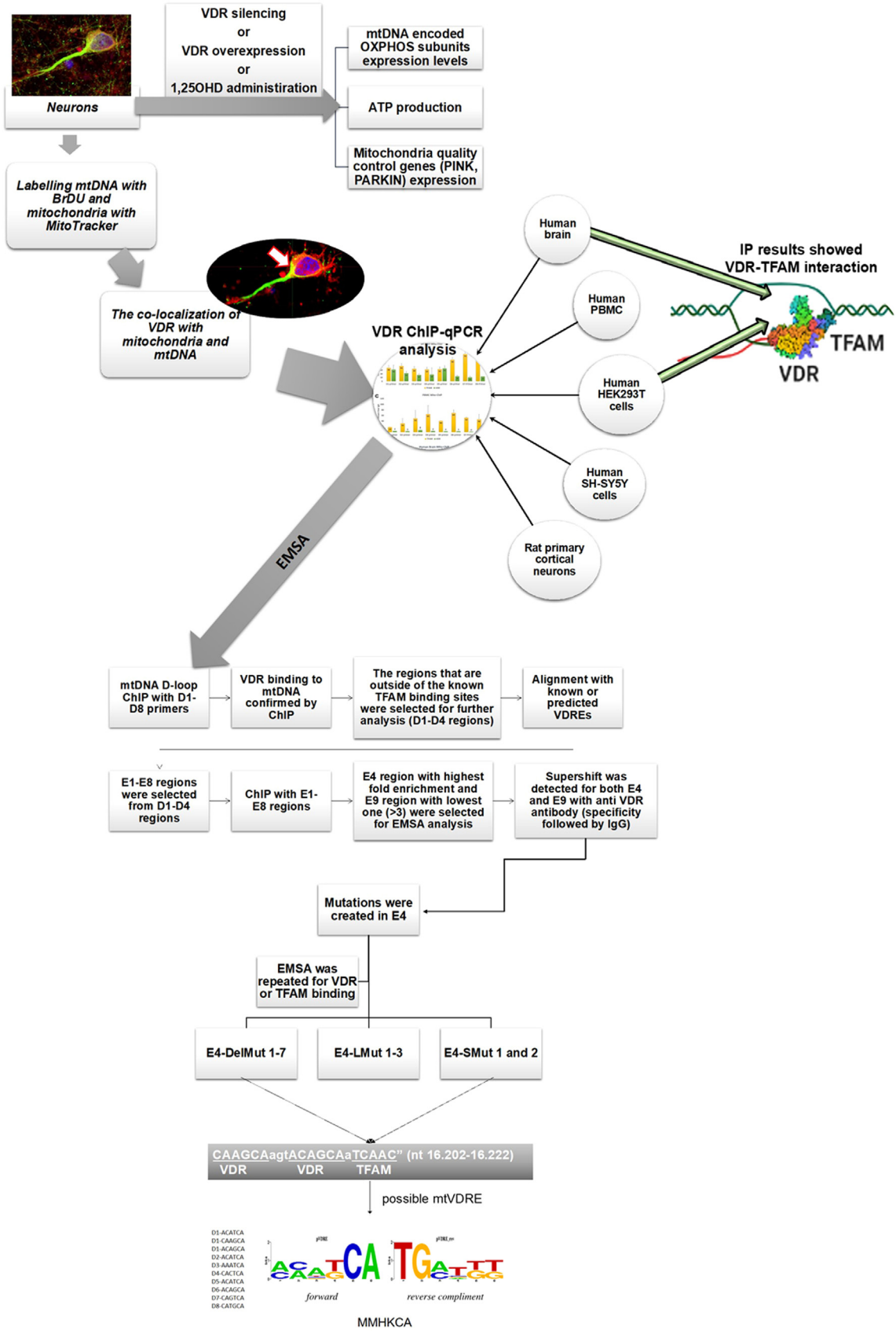

Fig. 1. The flow chart of methods performed in the present study and the steps of EMSA.

of the differentiation medium was replaced every 2–3 d. In addition, VDR overexpression and 1,25-dihydroxyvitamin D_3 treatments were performed to confirm the regulatory effects of VDR and vitamin D3 on mitochondrial genes since VDR is suggested to work in PC12 cells differently than other cells

2.1.4. SH-SY5Y cultures

SH-SY5Y cells (ATCC, CRL-2266) were cultured as previously described [13]. Briefly, the cells were plated in DMEM media containing 2 mM L-glutamine and 10% FBS and were incubated at 37°C and 5% CO_2 in a humidified atmosphere.

2.1.5. Peripheral mononuclear blood cells (PBMCs) isolation

PBMCs are collected from 12 healthy individuals whose ages range from 44 to 77 and are free from any neurodegenerative disorders. PBMCs were isolated from peripheral blood samples by density gradient separation as previously described [22]. Briefly, 3 mL of whole blood was layered onto the Histopaque-1119 and centrifuged for 30 min at 400 × *g*. Then, an opaque interface containing PBMCs was transferred into a clean centrifuge tube. PBMCs were washed with phosphate buffered-saline (PBS) twice with centrifugation at 250 × *g* for 10 min. PBMCs were resuspended in RPMI 1640 medium (Gibco, 21875-034) containing 15% FBS (Gibco, 10270-106), 1% antibiotic-antimycotic (Gibco, 15240-062), 1.5% phytohemagglutinin (Gibco, 10576-015), and 10% DMSO (Sigma, D8418) and stored in liquid nitrogen. Participants in the present study were treated according to the ethical principles for medical research involving human participants described in the World Medical Association's Declaration of Helsinki, and the study was approved by the Ethics Committee of Istanbul University-Cerrahpasa. Signed informed consent was obtained from all study participants.

2.1.6. Human brain samples

The human brain samples were taken during the epilepsy surgery of three patients. Those patients underwent extensive work-up before surgery for drug-resistant epilepsy. They were diagnosed with mesial temporal lobe epilepsy (two left/one right) with radiological, electrophysiological, and clinical evidence. There were two male and one female patient with an age range of 25–44 years. All of them were operated by the same surgical team with the anteromesial temporal lobectomy technique. According to this technique, the anterior part of the lateral temporal lobe is resected before reaching the mesial temporal structures. Therefore, in the beginning of the surgical removal of the temporal lobe, a cubic centimeter of middle temporal gyrus that was radiologically proven to be normal was resected and freshly put in HBSS (Gibco 14065-049) with 5 mg/mL D-glucose (Sigma G7021) and 2% Penstrep (Sigma T-4333). Participants in the present study were treated according to the ethical principles for medical research involving human participants described in the World Medical Association's Declaration of Helsinki, and the study was approved by the Ethics Committee of Istanbul University-Cerrahpasa. Signed informed consent was obtained from all study participants.

2.2. Treatments on cells

2.2.1. 1,25-Dihydroxyvitamin D_3 preparation and treatment

1,25-Dihydroxyvitamin D_3 (Sigma, C-9756) was prepared, as previously described [15]. In order to determine the possible effect of vitamin D3 on the transcription of mtDNA, the primary cortical neurons were treated with two different doses of 1,25OHD (10^{-7} M or 10^{-8} M) at two different time points (24 or 48 h). The doses and treatment periods were determined according to our previous works [10,15-20,24]. After the administration, total RNA was isolated at specific time points by using the PureLink RNA isolation kit (Ambion, 12183018A) according to the manufacturer's protocol, and the relative expression levels of mRNAs were determined.

Vehicle groups were established by treating the cells with ethanol, the solvent of 1,25 dihydroxyvitamin D3.

2.2.2. VDR silencing by siRNA treatment

VDR was silenced in primary neurons, as previously described [18,24]. Cyclophilin B siRNA-treated cells were used as the positive control, while cells treated with non-target siRNA were used as the negative control. The transfection reagent-treated cells were also used as control groups along with the untreated cells. RNA isolation was performed for all groups at 24 h and 48 h of the treatments.

2.2.3. VDR overexpression and 1,25-dihydroxyvitamin D3 treatment

The vitamin D receptor gene (NM_017058) was overexpressed in both primary neurons and differentiated PC12 cells by transfection with VDR Rat Tagged ORF Clone plasmid (OriGene, RR209091). As a negative control, the cells were transfected with a mammalian vector with C-terminal Myc-DDK Tag plasmid (OriGene, PS100001), which includes no open reading frame (ORF) for any gene and is thus referred to as a mock plasmid. This plasmid was used to distinguish between mimicry, inhibitory/activatory effects, and actual effects caused by transfection with VDR plasmid. Untreated cells were also used as an additional control group. Before the transfection, all culture mediums were replaced with Opti-MEM (Gibco, 51985). Plasmids were diluted in Opti-MEM at 1:250 (μg/μL), and a lipid-based transfection reagent, TurboFectin 8.0 (OriGene, TF81001) according to the manufacturer's protocol. The cells were incubated with prepared transfection reagent and plasmid complex for 24 h at 37°C and 5% CO_2 in a humidified incubator. After 24 h of transfection, Opti-MEM was replaced with a fresh culture medium.

Different treatment periods for VDR overexpression were tested for neurons and PC12 cells. As a result, 48 h for PC12 cells and 72 h for primary neurons were the most convenient time for efficient VDR overexpression.

We included two additional groups in VDR overexpression experiments: the 1,25 dihydroxyvitamin D_3 treatment group to observe the effect of vitamin D3 solely and the VDR overexpression+1,25 dihydroxyvitamin D_3 combined treatments group to inspect the effect of the ligand-substrate complex together. Both primary neurons and PC12 cells were treated with 10^{-8} M 1,25 dihydroxyvitamin D_3 for 24 or 48 h. However, the time courses of the treatment were different for these two types of cells. 1,25 dihydroxyvitamin D_3 application was performed at 24 h of the transfection in PC12 cells, while the same procedure was performed at 48 h of the transfection in neurons regarding the efficient VDR overexpression periods. RNAs were isolated in all groups at 48, 72, or 96 h of the treatments.

2.3. Cytotoxicity assay

The cytotoxicity levels of all groups were detected by a Cytotoxicity Detection kit (Roche, 11644793001) according to the manufacturer's protocol as previously described [15]. Measurements were done in triplicate for each sample, and the test was replicated.

2.4. mRNA expression analysis of mitochondrial genes

The mRNA expression levels of mitochondrial DNA-encoded OXPHOS complex subunits and nuclear DNA-encoded *PINK1* and *PARKIN* genes were determined by qRT-PCR from cultured neurons as previously described. RNA isolation was performed with a PureLink RNA Mini Kit (Thermo Fischer 12183018A) from cultured neurons. A fixed amount of RNA was set to 60 ng/μL for each sample during the cDNA synthesis reaction with the iScript cDNA synthesis kit (BioRad, 1708891). mRNA expression levels of NADH dehydrogenase subunits (*MT-ND1, MT-ND2, MT-ND3, MT-ND4, MT-ND4L, MT-ND5, MT-ND6*), cytochrome b (*MT-CYB*), cytochrome c oxidase subunits (*MT-CO1, MT-CO2, MT-CO3*), ATP synthase membrane subunits (*MT-ATP6, MT-ATP8*), *PINK1* and *PARKIN* were analyzed by qRT-PCR using specific LNA primers (Exiqon) and ExiLERATE LNA qPCR SYBR Green master mix kit (Exiqon, 303410) with a LightCycler 480 II Instrument (Roche Applied Biosystems). Actin beta (*ACTB*) (Exiqon, 308001), phosphoglycerate kinase 1 (*PGK1*) (Exiqon, 308004), and glyceraldehyde-3-phosphate dehydrogenase (*GAPDH*) (Exiqon, 308005) genes were used as reference genes. Catalog numbers of target and reference genes were given in Supplementary Table 1. Each qRT-PCR was performed in triplicates for a single experiment, and each experiment was repeated three times independently.

2.5. Investigating the cellular expression of VDR and OXPHOS subunits by immunofluorescent labeling

Rabbit polyclonal antibody to VDR-ChIP grade (ab3508, Abcam) specificity, which was used in immunofluorescent labeling, IP, and MitoChIP methods, was previously checked with silencing of *VDR* expression via siRNA treatment in our studies [24]. Our study indicated an almost 70% decrease in VDR immunolabeling in VDR silenced neurons [24]. It was also consistent with mRNA and western blot results in our several studies [16,18,24].

The expression of VDR protein was determined by immunofluorescent labeling to define the silencing efficiency or the over expression rate for the *VDR*. The expression of *MT-ND1, MT-ND4, MT-CO1, MT-CO2,* and *MT-ATP8* protein was determined by immunofluorescent/double immunoflourescent labeling to confirm mRNA expression results. Immunofluorescent labeling studies were performed as previously described [13,19]. Briefly, the cells were fixed with 3.7% paraformaldehyde (pH 7.4) and blocked with 30% goat serum in 0.02% T-PBS for 1 h at room temperature. Cells were then incubated with primary antibodies overnight at 4°C. On the second day, they were further processed with corresponding secondary antibodies labeled with Alexa Fluor in the dark for 1 h at room temperature. If it is double immunoflourescent labeling after fixation, blocking, and labeling with the first primary antibody, another blocking step with 10% goat serum was performed. Blocking was then followed by incubation with the second primary antibody for 2 h at room temperature. Cells were then labeled with corresponding secondary antibodies tagged with Alexa Fluor. Primary antibodies for immunofluorescent labeling were as follows: rabbit polyclonal antibodies to VDR-ChIP grade (Abcam, ab3508, dilution 1:100), MT-ND1 (ThermoFisher, PA5-75179, dilution 1:100), MT-ND4 (ThermoFisher, PA5-76458, dilution 1:200), MT-ATP8 (ThermoFisher, PA5-75605, dilution 1:100), mouse monoclonal antibodies to MT-CO1 [1D6E1A8] (Abcam, ab14705, dilution 1:200), MT-CO2 [12C4F12] (ThermoFisher, A-6404, dilution 1:100). Corresponding secondary antibodies were labeled with Alexa Fluor 488 (ThermoFisher, A11034, dilution 1:200) or AlexaFluor 568 (Abcam, ab175471, dilution 1:200). Images were acquired with Lionheart FX Automatic Fluorescent Microscope (Biotek) using Gen5 (Biotek) software. Negative control of immunofluorescent labeling was

also performed by omitting primary antibodies. The expression levels of target proteins were analyzed according to immunofluorescent intensities as described in the statistics section.

2.6. Mitochondrial localization of VDR

The localization of VDR in mitochondria was shown by fluorescent staining of mitochondria and immunofluorescence labeling of VDR in untreated primary neurons and SH-SY5Y cells. Initially, mitochondria were labeled with a mitochondrial membrane potential-sensitive fluorescent dye in live cells. Briefly, the culture medium was changed with Mitotracker Red CMXRos dye solution (ThermoFisher, M7512) diluted in HBSS (ThermoFisher, 14065056) and the cells were incubated at 37°C for 15 min. After the incubation, the staining solution was removed, and the cells were washed three times with PBS. Cells were then immunolabeled with rabbit polyclonal antibody to VDR-ChIP grade (Abcam, ab3508) as described above. Images were acquired with Leica TCS SP8 confocal microscope using LasX software or with Lionheart FX Automatic Fluorescent Microscope (Biotek) using Gen5 (Biotek) software.

2.7. Mitochondrial DNA and VDR co-localization

The co-localization of VDR with mitochondrial DNA (mtDNA) was determined by 5-bromo-2-deoxy-uridine (BrdU) labeling in untreated primary neurons and SH-SY5Y cells. BrdU is a thymidine analog and joins DNA while it is being synthesized. In this way, it enables the marking of newly synthesized DNA chains [52].

The cells were pretreated with aphidicolin (Sigma, A0781) with a final concentration of 20 μM for 60 min to inhibit nuclear DNA replication. Cells were incubated at 37°C and 5% CO_2 in a humidified incubator. After pretreatment, cells were treated with 15 μM BrdU (ThermoFisher, B23151) for 72 h at 37°C and 5% CO_2. Cells were then fixed with 3.7% paraformaldehyde. They were washed with PBS and then permeabilized with 0.1% TPBS for 20 min. The BrdU epitope was exposed by incubating the cells in 1N HCl on ice for 10 min and then in 2N HCl at room temperature for 10 min. The acid was neutralized by with phosphate/citric acid buffer (pH 7.4) incubation for 10 min. After washing with 0.1% TPBS, the cells were incubated with mouse monoclonal anti-BrdU primary antibody (ThermoFisher, B35128) at a dilution of 1:100 in 0.1% TPBS containing 5% goat serum and incubated overnight at room temperature. The next day the cells were incubated with AlexaFluor 488 tagged secondary antibody (ThermoFisher, A28175, dilution 1:200) for 1 h. After BrdU labeling, VDR was immunolabeled to determine the colocalization with mtDNA.

2.8. Mitochondrial chromatin immunoprecipitation (MitoChIP)

Mitochondrial chromatin immunoprecipitation (MitoChIP) was performed in primary cortical neurons, HEK-293T, SH-SY5Y cells, PBMCs of healthy human subjects, and human brain tissue. It included the following steps: 1) Isolation of mitochondria (~2×10^7 cells or ~200 mg brain tissue), 2) ChIP from isolated mitochondria, 3) qRT-PCR of samples for known mtDNA target sequences. Immunoprecipitations were carried out with an anti-VDR antibody as the target, an anti-TFAM antibody as a positive control, normal rabbit IgG, and an anti-ICAM antibody as negative controls.

Primary cortical neurons or HEK 293-T or SH-SY5Y cells were washed with PBS once and collected by scraping. PBMC cells of 12 healthy subjects were pooled for mitochondria isolation. All cells were centrifuged at 850x g. Mitochondria were isolated with ice-cold PBS and a protease inhibitor cocktail (ThermoFisher, 78425) from 200 mg of brain tissue. Mitochondria were isolated from the cell pellet with Mitochondria Isolation Kit for Cultured Cells (ThermoFisher, 89874) using a reagent-based method according to the manufacturer's protocol. mtDNA and mitochondrial proteins were cross-linked with 1% formaldehyde at room temperature for 10 min from isolated mitochondrial pellets. The crosslinking reaction was quenched by adding 0.125 M glycine, and the mitochondrial pellets were incubated for an additional 5 min at room temperature. The cross-linked mitochondrial pellet was washed twice with PBS. Mitochondrial DNA fragmentation was carried out with micrococcal nuclease enzyme at 37°C for 15 min by using a chromatin prep module (ThermoFisher, 26158) according to the manufacturer's protocol. The mitochondrial pellet was lysed in 2% CHAPS (ThermoFisher, 28300) prepared in Tris-buffered saline (ThermoFisher, 28379) supplemented with protease phosphatase inhibitor cocktail (ThermoFisher, 78443) and centrifuged at maximum speed for 2 min. The supernatant was collected into a new tube and diluted with ChIP dilution buffer (16.7 mM Tris–HCl, pH 8.1, 150 mM NaCl, 0.01% SDS, 1.1% Triton X-100, 1.2 mM EDTA). The mitochondrial lysate was precleared for 1 h at 4°C with ChIP grade A/G agarose beads (ThermoFisher, 26159) to eliminate non-specific bindings.

Rabbit polyclonal antibody to VDR-ChIP grade (Abcam, ab3508), rabbit polyclonal antibody to TFAM-ChIP grade (ThermoFisher, PA5-27865), rabbit IgG isotype control (ThermoFisher, 02-6102), or mouse monoclonal antibody to ICAM (Abcam, Ab20144) was added to the lysate and incubated at 4°C overnight. ChIP grade agarose A/G beads were added, and immunocomplexes were precipitated at 4°C for 4 h. The immunoprecipitants were sequentially washed twice with low-salt buffer (0.1% SDS, 1% Triton X-100, 2 mM EDTA, 20 mM Tris–HCl, pH 8.1,150 mM NaCl), high-salt buffer (0.1% SDS, 1% Triton X-100, 2 mM EDTA,20 mM Tris–HCl, pH 8.1, 500 mM NaCl), lithium chloride buffer (0.25 M LiCl, 1% Nonidet P-40, 1% deoxycholate, 1 mM EDTA, 10 mM Tris–HCl, pH 8.1) and TE (10 mM Tris, 1 mM EDTA). Immunoprecipitants were eluted with elution buffer (1% SDS and 0.1 M $NaHCO_3$) for 15 min twice. Reverse crosslink of protein-DNA complexes was performed by heating at 65°C in elution buffer with 0.2 M NaCl. Proteins were removed by incubating with proteinase K (ThermoFisher, 26160) for 2 h at 56°C. RNA molecules were removed by incubating with RNAaseA (ThermoFisher, 12091021) for 30 min at 37°C. DNA extraction was achieved with phenol:chloroform:isoamylalcohol (25:24:1) method. DNA was precipitated with two volumes of absolute ethanol and 0,5 M of ammonium acetate at −20°C overnight. ChIP DNA was analyzed by qRT-PCR method. DNA obtained before precipitation was collected and used as the input. The input was used for PCR evaluation. qRT-PCR was performed by using the PowerUp SYBR Green kit (ThermoFisher, A25742) according to the manufacturer's protocol using LightCycler 480 II Instrument (Roche Applied Biosystems). The locations and the sequences of the primer pairs corresponding to human mtDNA and corresponding to rat mtDNA used for MitoChIP are listed in Supplementary Figure 1, Supplementary Material 1–3. We used eight primer pairs to analyze the VDR interactions with mtDNA in the D-loop region. We designed D1 and D5 primers to include the possible VDRE sites on mtDNA that were suggested by Consiglio et al., with an *in silico* analysis [49]. The sequence information of D2-D4 and D6-D8 primers was used from a previous publication by Park et al. [53]. The D7 primer pair includes LSP, a known binding site for TFAM, D8 primer pair corresponds to the HSP2 promoter. One primer pair for the 16s rRNA coding region was used as a random primer. A nuclear-DNA coding housekeeping gene RpL13A was used as a negative control to check nuclear DNA contamination. Before EMSA experiments, further ChIP-qRT-PCR analyses were done with E1-E9 primers (Supplementary Material 1) to choose appropriate sequences for EMSA; a detailed explanation is given in the EMSA results section. Additional qRT-PCR that follows ChIP was performed with 18 primers that cover some parts of mtDNA (outside of the D-loop) [53] in HEK293T cells to understand the binding ability of VDR to other parts of mtDNA.

The fold enrichment values were calculated as relative folds over IgG with the $2^{\Delta\Delta Ct}$ method. Initially, ΔCt was calculated as the difference between the Ct values of the input and the immunoprecipitated sample. Subsequently, the ΔΔCt values were calculated by subtracting the ΔCt value of the non-specific negative control IgG (or no antibody sample) from the ΔCt value of the target sample that is immunoprecipitated with VDR, TFAM or ICAM antibody [54–57].

2.9. Co-immunoprecipitation (Co-IP)

HEK 293-T cells were washed with ice-cold PBS and scrapped with lysis buffer (150 mM NaCl, 50 mM Tris, 0.5 mM EDTA, 1% Triton-X 100), supplemented with a protease inhibitor cocktail (ThermoFisher, 78430) and incubated at 4°C for 30 min, followed by centrifugation at maximum speed at 4°C for 15 min. Approximately 200 mg of brain samples were washed with ice-cold PBS and then homogenized in IP lysis buffer. Homogenized brain samples were then incubated at 4°C for 1 h and centrifuged at maximum speed at 4°C for 30 min. Equal volumes of lysates were precleared with sepharose G beads (Sigma, P3296) at 4°C for 1 h of incubation, followed by centrifugation at 8,000 × *g* for 5 min at 4°C. Supernatants were collected into new tubes and treated with rabbit polyclonal antibody to VDR-ChIP grade (Abcam, ab3508), rabbit polyclonal antibody to TFAM-ChIP grade (ThermoFisher, PA5-27865). As a negative control, rabbit IgG isotype control (ThermoFisher, 02-6102) was added to the precleared lysates, and samples were incubated at 4°C overnight. Protein-antibody complexes were then incubated with sepharose G beads and precipitated via centrifugation at 6,000 × *g* for 3 min at 4°C. The precipitates were washed with PBS several times and analyzed by western blot. Complexes were eluted with 4X SDS-PAGE sample buffer containing %10 β-mercaptoethanol and were boiled at 100°C for 5 min. Proteins were separated from beads by boiling and centrifuging at 20,000 × *g* for 1 min. Protein samples were run in SDS-polyacrylamide gels (BioRad, 4561044) and then transferred onto PVDF membranes (BioRad, 1704272). Membranes were then blocked with 5% dry milk for 1 h at room temperature and incubated with VDR primary antibody at a dilution of 1:300 or TFAM antibody at a dilution of 1:800 or GAPDH primary antibody (Proteintech, 60004-1-Ig) at a dilution of 1:1,000 overnight at 4°C. GAPDH was not expected to interact with either TFAM or VDR and was used as a negative control for labeling. On the second day, membranes were incubated with HRP-conjugated VeriBlot for IP Detection Reagent (abcam, ab131366) at a dilution of 1:2,000 for 1 h at room temperature. The signals were detected by WesternBright ECL HRP substrate (Advansta, K-12045-D50) and were visualized by MicroChemi 4.2 MP (DNR BioImaging Systems).

2.10. Electrophoretic mobility shift assay (EMSA)

The rationale for EMSA and its steps are summarized in Figure 1. HEK293T cells transfected with VDR (NM_000376) Human Tagged ORF Clone plasmid

(Origene, RC209262) by TransIT-293 (Mirus, 2700) transfection reagent. The cells were treated with 10^{-8} mM 1,25OHD (Sigma, G9756), at 48 h of the transfection. Total cellular proteins used in EMSA were extracted by using M-PER Mammalian Protein extraction reagent (Thermo Scientific, 78501) including 10% Halt Protease Inhibitor (Thermo Scientific, 78429) and phosphatase inhibitor (Roche, 04906845001), at 72 h of the transfection. Protein concentration was determined in nanodrop by absorbance at 280 nm. Then, the samples were dialyzed with a mini dialyze device (ThermoFisher, 69550) in 220 mM NaCl. Target and mutant oligonucleotides (detailed sequence information was given in Table 1) were synthesized as single-stranded and biotinylated from the 3′-end of them with biotin 3′ end DNA labeling kit (ThermoFisher, 89818) following the manufacturer's protocol. The biotinylated single-stranded polymers were then annealed in a thermal cycler with a setting gradually reduced temperature from 94 to 25°C every 1 min.

The EMSA was performed using the LightShift EMSA Optimization and Control Kit (ThermoFisher, 20148X) according to the manufacturer's protocol. Briefly, 100 fmol of biotinylated double-stranded oligonucleotides were added to binding reactions containing binding buffer (10 mm Tris, 50 mm KCl, 1 mM DTT), 1% glycerol, 1 ug/uL poly(dI-dC) and 13 μg total protein extract in a total volume of 20 μL. Samples were incubated at RT for 20 min. For competition assays, an 800-fold molar excess of unlabeled oligonucleotides was added to the binding reaction before the addition of the biotinylated probe. The specificity of VDR-probe binding was confirmed by supershift assay. For supershift assays, 3.5 μg of VDR antibody (Abcam, ab3508) or anti-TFAM antibody (ThermoFisher, PA5-27865) were added to the binding reaction mixtures after 20 min of incubation, and the mixtures were incubated at RT for 50 min. The samples were mixed with 30% glycerol in PBS in a 6:1 sample: glycerol ratio and loaded on 4–20% non-denaturing TBE polyacrylamide gels (ThermoFisher, EC6225BOX). Electrophoresis was performed in 0.5× TBE buffer at 4°C for 10 min each at 100, 200, 400, and 500 mV, respectively. After electrophoresis, the samples were transfered onto nylon membranes (Thermofisher, 77016) with Trans-Blot Turbo Transfer System (Biorad) and crosslinked under UV light for 15 min. The biotinylated probes were detected using LighshiftChemiluminesecent EMSA Kit (ThermoFisher, 20148) according to the manufacturer's protocol. The nylon membranes were visualized by MicroChemi 4.2 MP (DNR Bio-Imaging Systems, Israel). Each EMSA was repeated at least three times independently.

2.11. Statistical analysis

Ct values obtained from qRT-PCR were calculated as previously described [15,16,18]. Cytotoxicity levels were compared to control groups and calculations were performed as previously described [15–19]. Corrected total cell fluorescence (CTCF) was determined, and calculated as previously described [24,58,59]. Raw data for each group for each type of experiment were analyzed via one-way ANOVA followed by a Tukey-Kramer multiple comparisons test (MCT) when data were normally distributed or a Kruskal-Wallis test followed by Dunn's multiple comparisons test when data were not normally distributed in GraphPad InStat DTCG 3.06. $P<.05$ was considered statistically significant. The text and figure legends present all data as means (SD). The EMBL-EBI search and sequence analysis tools (Lalign, Needle, Matcher, T-Coffee) were used for alignment analysis [60]. STAMP tool was used for the prediction of possible vitamin D response element (VDRE) in mtDNA [61].

3. Results

3.1. Cytotoxicity assays

The lactate dehydrogenase (LDH) release was used to determine the overall cytotoxic effect of 1,25OHD treatment, short-term VDR silencing, and VDR overexpression on cell survival. The LDH levels were significantly decreased in response to 48 h of 10^{-7} M or 10^{-8} M 1,25 dihydroxyvitamin D3 (1,25OHD) treatment compared to untreated control and ethanol groups ($P<.05$). LDH release of untreated control was designated as 0%. LDH release of other groups was as follows: 10^{-7} M 1,25OHD: -9,2 ± 2; 95% CI −11.7- to −6.7; 10^{-8} M 1,25OHD: -12.5 ± 3; 95% CI −16.1 to −8.8; 10^{-7} M ethanol: 3.4 ± 1.8; 95% CI 1.2–5.7. There was no significant difference in LDH release within 24 h of siRNA treatment, whereas LDH release was increased in siRNA-treated groups after 48 h of treatment ($P<.05$). LDH release of untreated control was designated as 0%. LDH release of other groups was as follows: Vehicle: 4.4 ± 6.7; 95% CI −1.2 to 10.0; Non-target siRNA: 0.6 ± 4.6; 95% CI −3.6 to 4.8; CycB siRNA: 7.3 ± 7; 95% CI 1.4–13.1; VDR siRNA: 19.6 ± 6.7; 95% CI 14.5–24.7. These results were in line with our previous data [20,24]. LDH release significantly changed at 96 h of overexpression experiment between untreated control and Mock or Mock+10^{-8} M Ethanol groups ($P<.001$, $P<.001$, respectively), whereas no significant difference was found in untreated control and VDR overexpressing and/or 1,25OHD treated groups ($P>.05$) in primary cortical neurons. LDH release of untreated control was designated as 0%. LDH release of other groups was as follows: Mock: 10.1 ± 0.9; 95% CI 9.4–10.8; Mock+10^{-8} M Ethanol: 8.6 ± 2.1; 95% CI 7.0–10.2; VDR overexpressing group: 5.8 ± 0.5; 95% CI 5.1–6.4; 1,25OHD treated group: 7.1± 1.5; 95% CI 5.5–8.7; VDR overexpressing+1,25OHD treated group: 6.3 ± 1.6; 95% CI 4.9–7.6.

There was no significant difference in the LDH release of PC12 cells at 48 h of the VDR overexpression experiment, whereas LDH release was decreased at 72 h in the 10^{-8} M 1,25OHD treated VDR overexpressing group compared to mock ($P<.01$) and 10^{-8} M 1,25OHD treated group ($P<.001$), and in VDR overexpressing group compared to 10^{-8} M 1,25OHD treated group ($P<.01$). LDH release of untreated control was designated as 0%. LDH release of other groups was as follows: Mock: 1.1 ± 1.2; 95% CI 0.2–2.0; Mock+10^{-8} M Ethanol: 0.5 ± 2.1; 95% CI −1.7 to 2.7; VDR overexpressing group: -4.2± 4.7; 95% CI −7.8 to −0.5; 1,25OHD treated group: 2.8± 1.5; 95% CI 1.4–4.2; VDR overexpressing+1,25OHD treated group: -6.7± 1.0; 95% CI −7.4 to −5.8.

3.2. Results of mRNA expression analysis (summarized in Table 2)

3.2.1. 1,25-Dihydroxyvitamin D3 (1,25OHD) administration in primary cortical neurons

At 24 h of treatments, *MT-ND6* and *MT-ATP8* relative mRNA expression levels of 10^{-7} M or 10^{-8} M 1,25OHD treated groups were higher than that of the control group (for *MT-ND6* after MCT $P<.05$, $P<.05$, respectively; for *MT-ATP8*; after MCT $P<.05$, $P<.001$, respectively). *MT-ATP6* mRNA levels of 10^{-7} M or 10^{-8} M 1,25OHD treated groups were lower compared to the control group (after MCT $P<.01$, $P<.05$, respectively) (Supplementary Fig. 2).

At 48 h of treatments, *MT-ND1, MT-ND3, MT-CO1, MT-CO2, MT-ATP6,* and *MT-ATP8* mRNA expression levels increased in 10^{-8} M 1,25OHD treated groups compared to control (after MCT $P<.05$, $P<.05$, $P<.05$, $P<.01$, $P<.001$, $P<.05$, respectively). *MT-ND4L,* and *MT-ND5* mRNA expression levels of 10^{-7} M or 10^{-8} M 1,25OHD treated groups were higher than that of control groups (for *MT-ND4L* after MCT $P<.01$, $P<.001$, respectively; for *MT-ND5* after MCT $P<.01$, $P<.01$, respectively; for *MT-ATP6* after MCT $P<.01$, $P<.01$, respectively) (Supplementary Fig. 2).

Relative expression of *PINK1* mRNA significantly decreased compared to control only after 24 h of treatment for 10^{-8} M 1,25OHD (overall *P*value=.02; after MCT $P<.05$). *PARKIN* mRNA expression increased only in the 10^{-8} M 1,25OHD treated group at 24 h compared to the control and the 10^{-7} M 1,25OHD treated groups (PARKIN 24 h, overall *P*value <.0001; after MCT $P<.001$, $P<.001$, respectively) and at 48 h compared to the control (PARKIN 48 h overall *P*value <.02; after MCT $P<.05$) (Supplementary Fig. 2). The ethanol group was used as a vehicle in which corresponding mRNA levels did not change compared to untreated cells ($P>.05$).

After determining of the effect of vitamin D3 on the transcription of mtDNA encoding genes, we wanted to see whether vitamin D3 changes intracellular ATP levels of primary cortical neurons or not. At 24 h of treatments, the ATP level of the 10^{-8} M 1,25OHD group was significantly higher than the untreated control, ethanol, or 10^{-7} M 1,25OHD groups ($P<.05$, $P<.05$, $P<.05$, respectively), whereas ATP level of 10^{-7} M 1,25OHD was increased at 48 h compared to the untreated control, ethanol, or 10^{-8} M 1,25OHD groups ($P<.01$, $P<.001$, $P<.05$, respectively) (Supplementary Fig. 3).

According to the results of 1,25OHD treatments, 10^{-8} M 1,25OHD dose was chosen for further analysis.

Table 1
The wild type (WT) and mutant mtDNA sequences used in EMSA assays

Name	DNA Sequence (5'-3')	mtDNAcoordinates	Description
E4	ACCCAATCCACATCAAAACCCCCTCCCCATGCTTACAAGCAAGTACAGCAATCAACC	16166- 16222	WT (colored sequences are possible VDRE; yellow sequence represents TFAM binding region according to EMSA results)
E9	ACCCTATTAACCACTCACGGGAGCTCTCCATGCATTTGGTATTTTCGTCTGGGGG	16-70	WT (underlined sequences are possible VDRE)
E4-DMut1	ATCCACATCAAAACCCCCTCCCCATGCTTACAAGCAAGTACAGCAATCAA	E4 region	Deletion of red and yellow regions
E4-DMut2	ACCCAACCCCCTCCCCATGCTTACAAGCAAGTACAGCAATCAA	E4 region	Deletion of blue and yellow regions
E4-DMut3	ACCCCCTCCCCATGCTTACAAGCAAGTACAGCAATCAA	E4 region	Deletion of red, blue and yellow regions
E4-DMut4	ACCCAATCCACATCAAAACCCCTTACAAGCAAGTACAGCAATCAA	E4 region	Deletion of green and yellow regions
E4-DMut5	ACCCAATCCACATCAAAACCCCCTCCCCATGCT	E4 region	Deletion of gold and yellow regions
E4-DMut6	ATGCTTACAAGCAAGTACAGCAATCAA	E4 region	Deletion of red, blue and half of green region
E4-DMut7	ACCCAATCCACATCAAAACCCCCTCCCCATGCTTACAAGCAAGTCAA	E4 region	Deletion of half of gold region and yellow regions
E4-NMut1	ACCCAATCCCACTAAAAACCCCCTCCCCATGCTTAACCGATAGTCACGAAATCAACC	E4 region	Mutated nucleotides are shown in the boxes
E4-NMut2	ACCCAATCCCACTAAAAACCCCCTCCCCATGCTTACAAGCAAGTCACGAAATCAACC	E4 region	Mutated nucleotides are shown in the boxes
E4-NMut3	ACCCAATCCCACTAAAAACCCCCTCCCCATGCTTAACCGATAGTCACGAAAGCCCAA	E4 region	Mutated nucleotides are shown in the boxes
E4-DivNMut1	CATGCTTAAACTAAAGTACAGACATCAAC	E4 region	Mutated nucleotides are shown in the boxes
E4-DivNMut2	CATGCTTAAACTAAAGTACAGCAATCAAC	E4 region	Mutated nucleotides are shown in the boxes
Human 24 hydorxylase VDRE	AGGCCCGGACGCCCCTCGCTCACCTCGCTGACTCCATCCTCCTT	-	WT , Containing the VDRE sequence

DMut:Deletion Mutant , NMut : Nucleotide Exchange mutant DivNMut: Divided Sequence Nucleotide Exchange mutant

3.2.2. VDR silencing by siRNAs in primary cortical neurons

After determining the 1,25 OHD effect on the mRNA expression of mtDNA encoding genes, the major receptor of 1,25OHD, *VDR*, was silenced at 24 or 48 h in primary cortical neurons to understand the mechanism of transcription regulation by 1,25OHD. The silencing of *VDR* was confirmed by qRT-PCR and IF labeling (Fig. 2A–D), and the silencing efficiency was similar to our previous studies [18,19,24]. According to our experience, 24 h of *VDR* silencing creates a response in target mRNAs, and the most significant results were gathered from 24 h of treatments.

At 24 h of administration, the relative expression levels of *MTND2, MTND4L, MT-CYB, MT-CO1, MT-CO2, MT-CO3*, or *MT-ATP6* mRNA in VDR siRNAs treated groups significantly decreased compared to control groups -untreated control, vehicle, non-target siRNA treated and CycB siRNA treated groups- ($P<0.05$). MT-ND5 mRNA expression was decreased compared to untreated control, vehicle, and non-target siRNA groups ($P<0.05$) except CycB siRNA group ($P>.05$) at 24 h of treatments, whereas its expression increased compared to non-target siRNA and CycB siRNA treated groups at 48 h of treatments ($P<.05$) (Fig. 2E). Detailed multiple comparison tests (MCT) results are given in Figure 2E.

Some OXPHOS complex subunits were selected for IF analysis (*MT-ND1, MT-ND4, MT-CO1, MT-CO2, MT-ATP8*) to understand whether the changes in their mRNA expressions are reflected in the protein levels. CTCF levels of corresponding proteins showed that the protein levels of these genes changed similarly to mRNA levels in response to VDR silencing, except *MT-ATP8*. The mRNA level of *MT-ATP8* did not change, whereas its protein level increased in response to VDR silencing (Supplementary Fig. 4).

Additionally, *PINK1* and *PARKIN* mRNA levels were also investigated in the VDR silencing experiment. PINK1 mRNA expression did not change, whereas *PARKIN* mRNA levels increased in VDR-silenced groups compared to control groups ($P<.05$) (Fig. 2E). Detailed multiple comparison tests (MCT) results are given in Figure 2E. All results were also summarized in Table 2.

3.2.3. VDR overexpression in primary cortical neurons and PC12 cells

In addition to *VDR* silencing, we wanted to confirm the effect of VDR on mtDNA encoding genes and *PINK1* and *PARKIN* by overexpression. In this experiment, we used another cell type, PC12, in addition to primary cortical neurons. The PC12 cell line was used as its vitamin D response was reported to be different from other cell types [62]. We thought that the difference might be originated from the *VDR* expression level of PC12, and before the experiments, the *VDR* mRNA levels of primary cortical neurons and PC12 cells were compared. We showed that the untreated primary cortical neurons express very high levels of *VDR* than untreated PC12 cells ($P=.002$) (Supplementary Fig. 5). Given the very low levels of VDR, VDR was not silenced but over-expressed in PC12 cells. Therefore, we used these two cell types to evaluate the vitamin D3/VDR effect in different neuronal cells to show whether the observed effect of vitamin D3/VDR is limited to only one cell type. The different responses of vitamin D3 in these two cell types were also confirmed after *VDR* transfection. A significant increase in *VDR* after plasmid transfection was determined at 72 h in primary cortical neurons (Fig. 2A–C) and 48 h in PC12 cells (Supplementary Fig. 5).

1,25OHD was added to the cell culture media considering the 1,25OHD treatment results, which showed the best responses in 10^{-8} M treated groups at 24 and 48 h. Therefore 10^{-8} M 1,25OHD was added to the culture before 24 h of the best transfection rate. For primary cortical neurons, it was added at 48 h of treatments, and total RNA was isolated at 72 and 96 h. For PC12 cells, it was added at 24 h, and total RNA was isolated at 48 and 72 h.

To distinguish between mimicry and inhibitory/activatory effects and true effect, the Mock group (empty plasmid) was used as a control for the VDR overexpression group, and the Mock+10^{-8} M Ethanol treated group was used as a control for 10^{-8} M 1,25OHD treated VDR overexpressing (VDR+10^{-8} M 1,25OHD) group. Only the changes between these groups were accepted as the effect of VDR and/or vitamin D3.

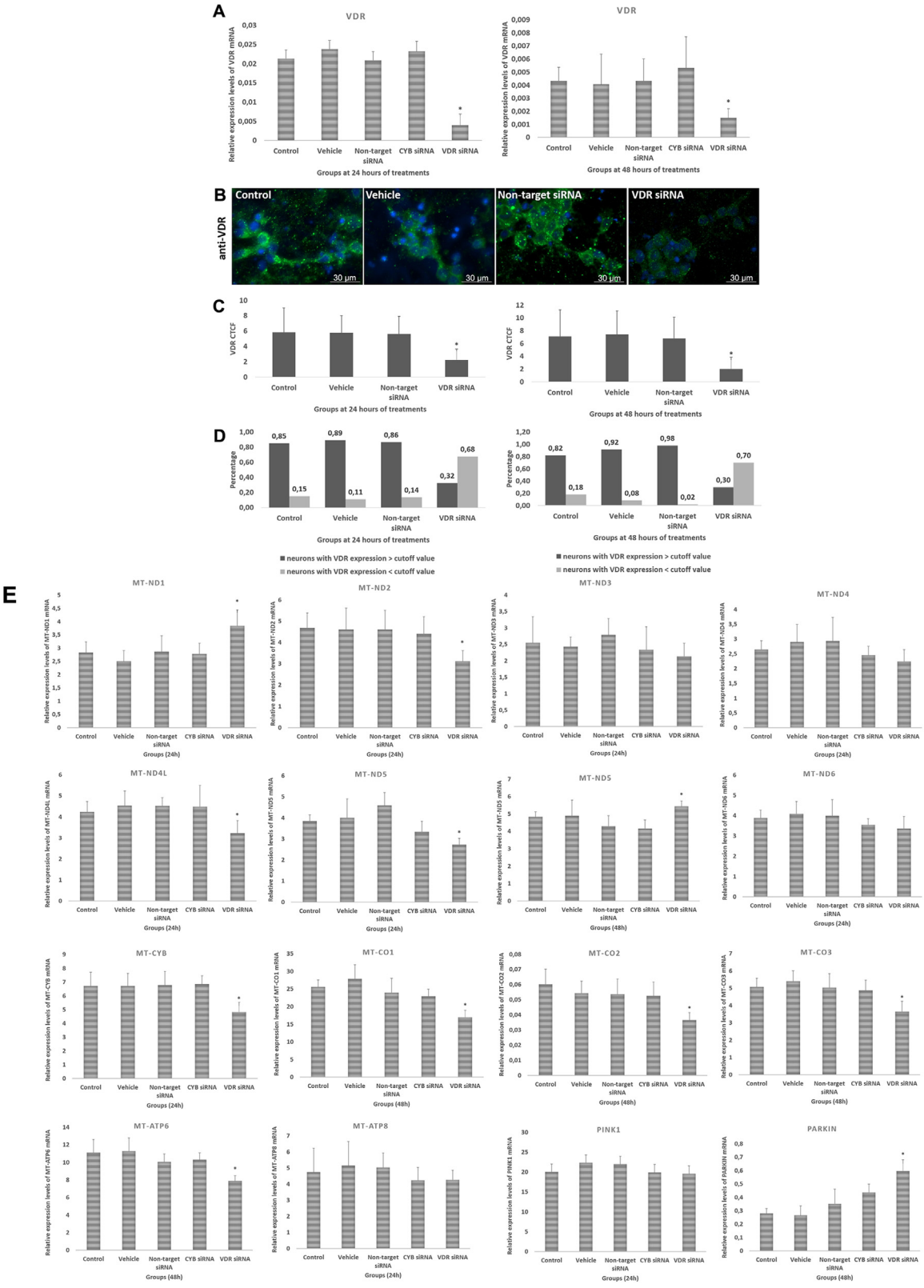

Fig. 2. Silencing verification of VDR siRNA experiment in primary cortical neurons after 24 and 48 h of treatments. (A) Relative expression levels of VDR mRNA at 24 or 48 h. *$P<.05$. (B) Immunofluorescent labeling of VDR (green). Magnification: 63×. (C) The corrected total cell fluorescence-CTCF of the VDR protein in control groups (untreated control, vehicle, non-target siRNA) and VDR siRNA-treated group after 24 or 48 h of treatments. The intensity of the VDR protein signal in the *VDR* siRNA treated group was significantly lower than in other groups in 24 and 48 h of treatments ($P<.001$). (D) The percentage of VDR-expressing neurons after 24 or 48 h of treatments. The percentage of neurons that expressed VDR at a level that was higher than the cutoff value (2.6; for 24 h and 2.4; for 48 h of treatments) were significantly lower in the VDR siRNA treated groups both in 24 h ($P<.0001$; χ^2: 125.6; df: 3) and the 48 h ($P<.0001$; χ^2: 80.9; df: 3) of treatments. Data are presented as the mean (SD). Control: untreated control group; vehicle: transfection reagent-treated control group; non-target siRNA: non-target siRNA-treated negative control group; *VDR* siRNA: *VDR* siRNA pool-treated group. (E)

3.2.3.1. VDR overexpression in primary cortical neurons. The overexpression of VDR was confirmed by IF labeling at 96 h (Fig. 3A–C). Untreated control, Mock (empty plasmid for VDR overexpression group), and Mock+10^{-8} M ethanol (for VDR overexpression+1,25OHD group) groups were used as controls.

MT-ND3, MT-ND4L, MT-ND5, MTCO1, and *MT-ATP8* mRNA levels significantly increased after VDR overexpression, and the expression elevation increased much more with 1,25OHD treatment to the VDR overexpressed group. Expression levels of *MT-ND6* mRNA did not change with *VDR* overexpression, but its level increased by 1,25OHD treatment. *MT-ND1, MT-ND4,* and *MT-CO2* mRNA levels increased only in the *VDR* overexpression+1,25OHD group. All the statistical analyses are given in Figure 2D. 1,25OHD treatment results of this experiment were in line with the results of the independent 1,25OHD administration experiment, which results were given above section and in Supplementary Figure 2.

PINK1 mRNA level decreased only with 1,25OHD at 72 h, whereas the *PARKIN* mRNA level increased corresponding to 1,25OHD and/or *VDR* overexpression at 96 h. The statistical analysis is given in Figure 3D.

Shortly, we showed that the *VDR* overexpression seems to be more effective with 1,25OHD administration on the expression of mtDNA encoding genes.

3.2.3.2. VDR overexpression in PC12 cells. The overexpression of *VDR* was confirmed at 48 and 72 h of treatments by qRT-PCR (Supplementary Fig. 5). Untreated control, Mock (empty plasmid for *VDR* overexpression group), and Mock+10^{-8} M ethanol (for *VDR* overexpression+1,25OHD group) groups were used as controls.

The mRNA expression levels of *MT-ND2* and *MT-ND6* increased with 1,25OHD and/or *VDR* overexpression compared to control groups, whereas *MT-ND4, MT-ND4L,* and *MT-CO1* levels decreased in the same way. *MT-ND1, MT-ND5, MT-CO3, MT-ATP6* mRNA levels decreased in response to 1,25OHD treatment. *MT-CO2* mRNA levels increased in response to *VDR* overexpression.

PINK1 mRNA level decreased with 1,25OHD and/or *VDR* overexpression. *PARKIN* mRNA level decreased corresponding to 1,25OHD and/or *VDR* overexpression at 48 h, but its level increased with 1,25OHD and/or *VDR* overexpression at 72 h. The statistical analysis is given in Supplementary Figure 5.

3.3. The co-localization of VDR with mitochondria and mtDNA

Considering the results presented above, and the fact that it is a secosteroid hormone and an essential TF for the nuclear genome, we thought that VDR might also interact with mitochondrial DNA. Therefore, we examined whether VDR localizes with mtDNA in primary cortical neurons, which we prevented DNA synthesis by aphidicolin treatment. To test this hypothesis, we performed a set of immunocytochemical experiments for VDR and BrdU, a thymidine analog, that allows us to visualize the co-localization of VDR and BrdU labeled mtDNA. First of all, the mitochondrial localization of VDR was confirmed by double labeling of MitoTracker red with VDR. Our results confirmed that VDR localizes into mitochondria (Fig. 4A–C). Next investigated the possible interaction between endogenous VDR and mtDNA. After incubation with BrdU, the cells were fixed and labeled with anti-BrdU antibody to visualize BrdU incorporation into DNA. For double labeling, cells were then treated with the anti-VDR antibody targeting endogenous VDR. BrdU-incorporated mtDNA was marked green, endogenous VDR was marked red, and the nuclear genome was marked with DAPI (Fig. 4A–C). As shown in the figure, our results show that endogenous VDR co-localized with BrdU-labeled mtDNA. In addition, these results were confirmed in another neuronal cell type, namely SH-SY5Y (Fig. 4C). These findings indicated that VDR could get inside mitochondria and co-localize with mtDNA in primary cortical neuron cells without any VDR overexpression or 1,25OHD treatment.

3.4. Mitochondrial DNA-chromatin immunoprecipitation (ChIP) with VDR

To further substantiate VDR-mtDNA interaction, after we showed the co-localization of endogenous VDR with mtDNA by immunofluorescence-based BrdU assay, we performed mitochondrial DNA ChIP experiments in primary cortical neurons, HEK293-T, SH-SY5Y cells, PBMCs or human brain tissue. Our results showed that there was no significant enrichment of input or any other precipitated samples on the Rpl13A gene, which was used as a control for nuclear DNA contamination, and the enrichment results was equal to non-specific IgG in all cell lines. These control results show that the ChIP experiment was done successfully for VDR or TFAM. VDR mtDNA-ChIP results for all different cell types are given below. In summary, VDR was found to bind the mtDNA D-loop region weakly in PBMC cells but very strongly in other cells, and the data were confirmed in human brain tissue.

3.4.1. HEK293T cells

The fold enrichment analysis of the mtDNA fragments that were pulled down with anti-VDR antibody showed that VDR binds to the D-loop region in the HEK293T cells. We observed strong signals in the 16,023–16,520 region corresponding to upstream of mtDNA heavy strand promoter (Figure 4D). Additionally, we compared mtDNA binding patterns of VDR and TFAM, which we used as a positive control, by using D-loop specific primer pairs (Fig. 4D) and 16s rRNA gene-specific primer (Supplementary Fig. 6). We observed that VDR-mtDNA binding pattern was similar to that of TFAM-mtDNA. The percentage input (% input) results were given in Supplementary Figure 6. In order to determine the specificity of TFAM or VDR ChIP, we used non-target ICAM antibodies and only bead samples as negative controls, in addition to non-specific IgG. The TFAM or VDR ChIP percentage input results were considerably higher than all negative controls (Supplementary Fig. 6).

3.4.2. SH-SY5Y cells

The fold enrichment analysis indicated that VDR associates with mtDNA D-loop regions that we investigated in the SH-SY5Y cells. VDR binding was weaker than TFAM around HSP and LSP promoters corresponding to D6-D8 primers. We observed that VDR bind-

The effect of VDR silencing on the mRNA expression of mtDNA encoding OXPHOS subunits and nuclear DNA encoding PINK1 and PARKIN in primary cortical neurons. The time points at which the data were significant or the data which are not significant at both time points are presented in the figure. The relative expression levels of *MT-ND1* (24 h), and *PARKIN* (48 h) were significantly increased in VDR siRNA treated groups (for MT-ND1 after MCT: $P<.05$, $P<.001$, $P<.05$, $P<.05$, respectively; for PARKIN after MCT: $P<.001$, $P<.001$, $P<.001$, $P<.05$, respectively). *MT-ND2* (24 h), *MT-ND4L* (24 h), *MT-CYB* (24 h), *MT-CO1* (48 h), *MT-CO2* (48 h), *MT-CO3* (48 h), *MT-ATP6* (48 h) were significantly decreased in *VDR* siRNA treated groups compared to control groups (for MT-ND2 after MCT: $P<.05$, $P<.05$, $P<.05$, $P<.05$, respectively; for MT-ND4L after MCT: $P<.05$, $P<.05$, $P<.05$, $P<.05$, respectively; for MT-CYB after MCT: $P<.05$, $P<.05$, $P<.05$, $P<.05$, respectively; for MT-CO1 after MCT: $P<.001$, $P<.001$, $P<.01$, $P<.05$, respectively; for MT-CO2 after MCT: $P<.001$, $P<.01$, $P<.05$, $P<.05$, respectively; for MT-CO3 after MCT: $P<.05$, $P<.001$, $P<.01$, $P<.01$, respectively; for MT-ATP6 after MCT: $P<.001$, $P<.001$, $P<.05$, $P<.01$, respectively). *MT-ND5* mRNA expression was decreased compared to untreated control, vehicle, non-target siRNA groups (after MCT: $P<.05$, $P<.05$, $P<.001$) except CycB siRNA group (after MCT: $P>.05$) at 24 h of treatments, whereas its expression increased compared to non-target siRNA and CycB siRNA treated groups at 48 hours of treatments (after MCT: $P<.05$, $P<.01$)*$P<.05$.

Table 2
The summary of the alterations of mRNA levels of mtDNA encoded genes in primary cortical neurons.

The alterations of mRNA levels of mtDNA encoded genes due to different treatments in primary cortical neurons				
Genes	Treatment type			Conclusion
	1,25OHD administration	VDR silencing by siRNA	VDR over-expression (with or without 1,25OHD)	
MT-ND1	Increased at 48 h	Increased (Confirmed at protein levels by IF)	Increased by 1,25OHD at 96 h and in VDR over-expression+ 1,25OHD group	1,25OHD presence is effective; VDR elevation or silencing has complex effects
MT-ND2	Not effected	Decreased	Not effected	1,25OHD presence or VDR elevation is ineffective; VDR silencing is effective
MT-ND3	Increased at 48 h	Not effected	Increased by VDR over-expression or 1,25OHD	1,25OHD or VDR elevation is effective; VDR silencing is ineffective
MT-ND4	Not effected	Not effected (Confirmed at protein levels by IF)	Increased only in the VDR over-expression+ 1,25OHD group	1,25OHD and VDR elevation are effective; VDR silencing is ineffective
MT-ND4L	Increased at 48 h	Decreased	Increased by VDR over-expression or 1,25OHD	All situations are harmoniously effective
MT-ND5	Increased at 48 h	Decreased at 24 h; Increased at 48 h	Increased by VDR over-expression or 1,25OHD	All situations are harmoniously effective
MT-ND6	Increased at 24 h	Not effected	Increased by 1,25OHD at 96 h and in VDR over-expression+ 1,25OHD group	1,25OHD and VDR elevation are effective; VDR silencing is ineffective
MT-CYB	Not effected	Decreased	Not effected	1,25OHD presence or VDR elevation is ineffective; VDR silencing is effective
MT-CO1	Increased at 48 h	Decreased (Confirmed at protein levels by IF)	Increased by VDR over-expression or 1,25OHD	All situations are harmoniously effective
MT-CO2	Increased at 48 h	Decreased (Confirmed at protein levels by IF)	Increased only in the VDR over-expression+ 1,25OHD group	All situations are harmoniously effective
MT-CO3	Not effected	Decreased	Not effected	1,25OHD presence or VDR elevation is ineffective; VDR silencing is effective
MT-ATP6	Decreased at 24 h; Increased at 48 h	Decreased	Increased by 1,25OHD at 96 h; Not effected by VDR over-expression	1,25OHD or VDR silencing is effective
MT-ATP8	Increased at 24 h and 48 h	Not effected (Increased at protein levels by IF)	Increased by VDR over-expression or 1,25OHD	1,25OHD and VDR elevation are effective; VDR silencing is ineffective
The alterations of mRNA levels of nuclear DNA encoded genes due to different treatments in primary cortical neurons				
PINK1	Decreased at 24 h	Not effected	Decreased by 1,25OHD at 72 h; Not effected by VDR over-expression	1,25OHD presence is effective; VDR elevation or silencing is ineffective
PARKIN	Increased at 24 h and 48 h	Increased	Increased by VDR over-expression or 1,25OHD	1,25OHD presence is effective; VDR elevation or silencing has complex effects

ing pattern to mtDNA was similar to that of TFAM on regions corresponding to D1 and D5 primers in SH-SY5Y cells (Fig. 4E).

3.4.3. Rat primary cortical neurons

ChIP was performed only once in rat primary cortical neurons because of the requirement of a large number of cells in the assay. However, results showed a strong binding pattern for VDR to D-loop corresponding sequences in rats and detailed results were given in Supplementary Material 3.

3.4.4. PBMC

The fold enrichment analysis of VDR-mtDNA pulldowns in human PBMC showed that VDR binds at 16,400–16,520 regions on mtDNA D-loop corresponding to primer set D3 (Fig. 4F). Additionally, this region showed a nearly two to fourfold higher VDR association when compared to the other regions. There was no significant VDR association at the D-loop region around mtDNA HSP and LSP sites. Also, we did not observe significant enrichment of VDR binding on 16s rRNA coding region (Supplementary Fig. 6). On the other hand, TFAM binding signals were observed to be at least

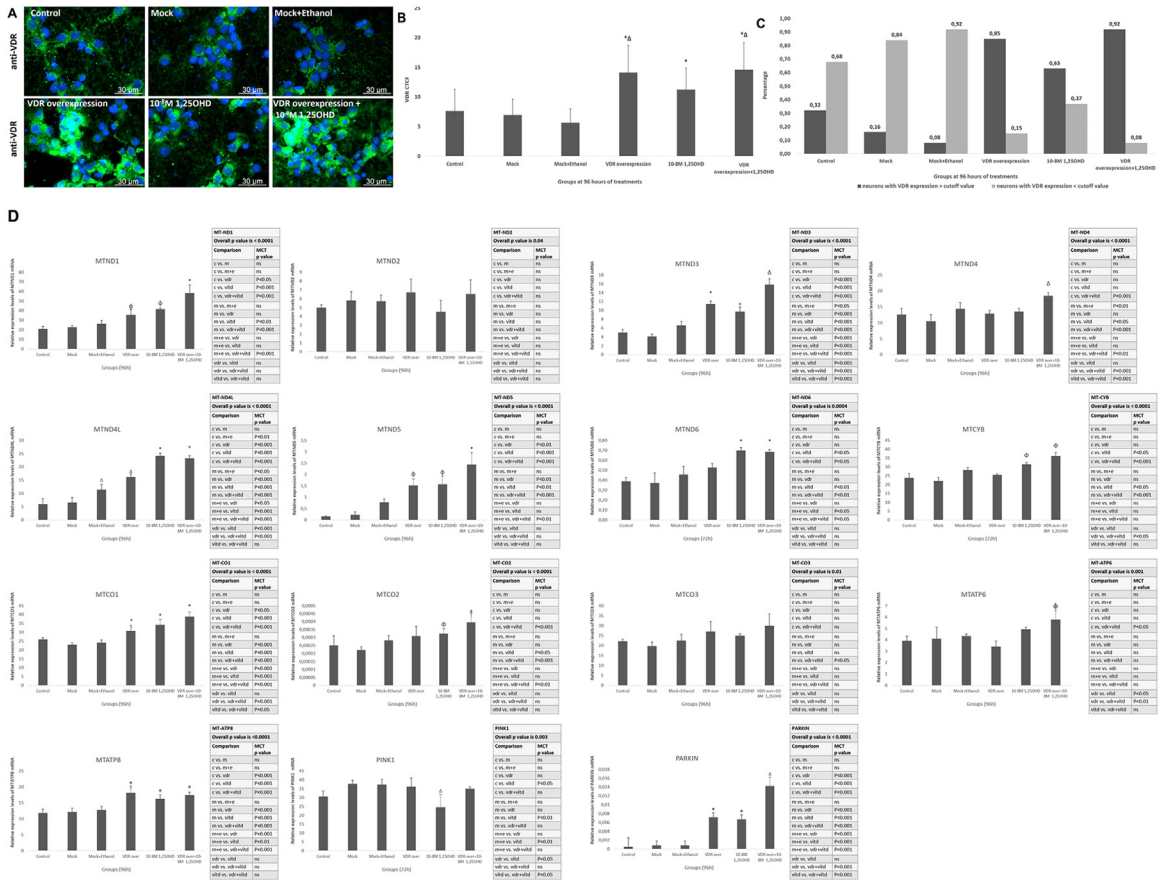

Fig. 3. Verification of VDR overexpression in primary cortical neurons. (A) Immunofluorescent labeling of VDR (green). Magnification: 63×. (B) The corrected total cell fluorescence-CTCF of the VDR protein in control groups (untreated control, mock, mock+ethanol) and treatment groups (VDR overexpressing, 10^{-8} M 1,25OHD treated and VDR overexpressing+ 10^{-8} M 1,25OHD treated groups) after 96 h of treatments. The intensity of the VDR protein signal in VDR overexpressing or VDR overexpressing+ 10^{-8} M 1,25OHD treated groups were significantly higher than in other groups ($P<.001$). The CTCF levels of 10^{-8} M 1,25OHD treated group was significantly higher than control groups ($P<.001$), whereas significantly lower than VDR overexpressing ($P<.05$) or VDR overexpressing+ 10^{-8} M 1,25OHD treated ($P<.01$) groups. (C) The percentage of VDR-expressing neurons after 96 h of treatments. The percentage of neurons that expressed VDR at a level that was higher than the cutoff value (9.8) was significantly higher in the VDR overexpressing, 10^{-8} M 1,25OHD treated, and VDR overexpressing+ 10^{-8} M 1,25OHD treated groups ($P<.0001$; χ^2: 281.2; df: 5). *Significant ($P<.05$) compared to all control groups, Δ Significant ($P<.05$) compared to all groups. (D) The effect of VDR overexpression and/or 10^{-8} M 1,25OHD treatment on the mRNA expression of mtDNA encoding OXPHOS subunits and nuclear DNA encoding PINK1 and PARKIN in primary cortical neurons. Only the time points at which the data were significant are presented in the figure. *Significant ($P<.05$) compared to all control groups, Φ Significant ($P<.05$) compared to control groups, ŧ Significant ($P<.05$) compared to experimental groups, Δ Significant ($P<.05$) compared to all groups.

fourfold higher than VDR binding on all regions. The specificity of TFAM/VDR ChIP in PBMCs was confirmed with % input. We also reported IgG and VDR/TFAM results as % input (Supplementary Fig. 6). The % input value of VDR ChIP in the region corresponding to the D3 primer was higher than IgG, confirming the fold enrichment analysis.

3.4.5. Human brain tissue

The fold enrichment analysis of human brain tissue samples also verified that VDR strongly binds to the D-loop region (Fig. 4G). We reported IgG and VDR/TFAM results as % input (Supplementary Fig. 6). Additionally, we observed significant enrichment of VDR binding on 16s rRNA coding region (Supplementary Fig. 6).

3.4.6. VDR mtDNA-ChIP assay for the regions outside of the D-loop

Consiglio et al. suggested the possible mtDNA VDREs in both the D-loop and outside of the D-loop region according to their *in silico* analysis [49]. Therefore, we conducted additional qRT-PCR following ChIP only in HEK293T cells. The qRT-PCR involved 18 primers covering most parts of mtDNA (outside of the D-loop) [53]. In addition, results showed that VDR is also able to bind mtDNA regions that are located outside of the D-loop (qRT-PCR results were given in Supplementary Material 2).

3.5. Electrophoretic mobility shift assay (EMSA) results

The interaction of VDR with target mtDNA sequences was determined by EMSA combined with supershift (supershift EMSA) (Fig. 5A–F). The workflow for EMSA was given in Figure 1.

3.5.1. Alignment analysis for known VDR-response elements

First, the sequences of the D-loop region were aligned to the defined/known VDR-response elements (VDREs) using alignment servers as mentioned in the statistical analysis section. After the alignments, the regions amplified by D5, D7, and D8 primers (Supplementary Fig. 1), including TFAM binding sites, were excluded from the analysis since we wanted to search specific binding sites for VDR-independent from TFAM binding sites.

3.5.2. Determination of smaller mtDNA fragments that will be used in EMSA

According to SH-SY5Y ChIP results, four target regions (D1-strong binding, D2-mild binding, D3, and D4-weak binding) were

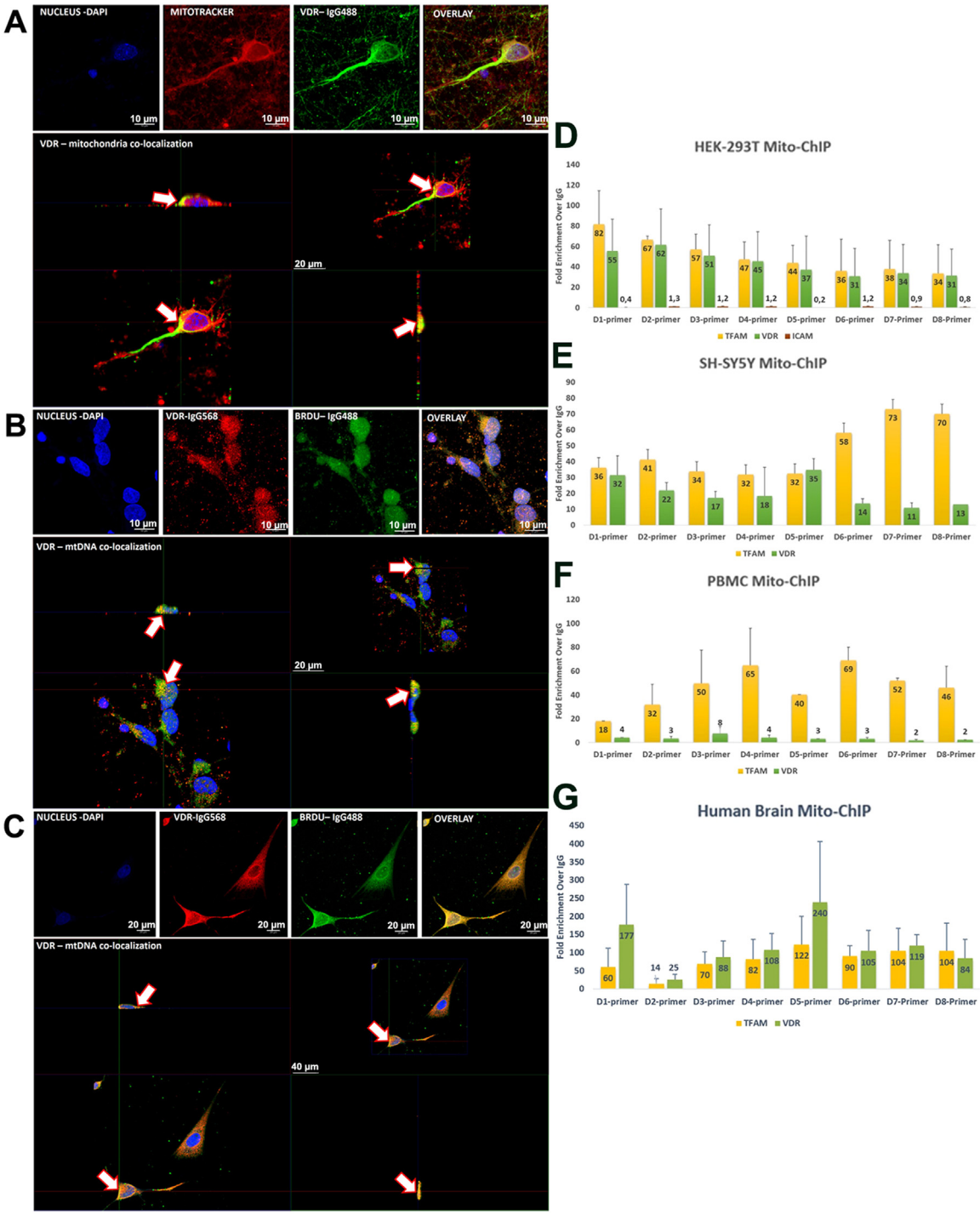

Fig. 4. The colocalization of VDR with mitochondria and the mtDNA. (A) The colocalization of VDR with mitochondria in primary cortical neurons. The upper row presents separated channels: Nucleus (blue, staining: DAPI), Mitochondria (red, staining: Mitotracker Red CMXRos dye solution), VDR (green, labeling: anti-VDR antibody+alexafluor 488 tagged secondary antibody), and the overlay image. The lower row presents the image's cross-section: The yellow pixels marked with an arrow indicate the colocalization of VDR with mitochondria. Magnification: 63×. (B) The colocalization of VDR with mtDNA in primary cortical neurons. The upper row presents separated channels: Nucleus (blue, staining: DAPI), VDR (red, labeling: anti-VDR antibody+alexafluor 568 tagged secondary antibody), mtDNA (green, labeling: anti-BrdU antibody+alexafluor 488 tagged secondary antibody), and the overlay image. The lower row presents the image's cross-section: The yellow pixels marked with an arrow indicate the colocalization of VDR with mtDNA. Magnification: 63×. (C) The colocalization of VDR with mtDNA in SH-SY5Y cells. The upper row presents separated channels: Nucleus (blue, staining: DAPI), VDR (red, labeling: anti-VDR antibody+alexafluor 568 tagged secondary antibody), mtDNA (green, labeling: anti-BrdU antibody+alexafluor 488 tagged secondary antibody), and the overlay image. The lower row presents the image's cross-section: The yellow pixels marked with an arrow indicates the colocalization of VDR with mtDNA. Magnification: 63×. (D) Mitochondrial chromatin immunoprecipitation (MitoChIP). HEK-293T MitoChIP: Fold enrichment analysis indicated an almost identical binding pattern for both VDR and TFAM to mtDNA in HEK-293T cells. (E) SH-SY5Y MitoChIP: VDR and TFAM bind to mtDNA in SH-SY5Y cells. The binding capacity of VDR to mtDNA seems lesser for D6, D7, and D8 sites. The same sites have a higher affinity to TFAM. (F) PBMC MitoChIP: the most probable site that VDR binds on mtDNA is the D3 site. % input results for selected primers were given in Supplementary Figure 6. (G) Human brain MitoChIP: VDR and TFAM bind to mtDNA in human brain samples of three individuals. VDR binding ability to mtDNA is very strong.

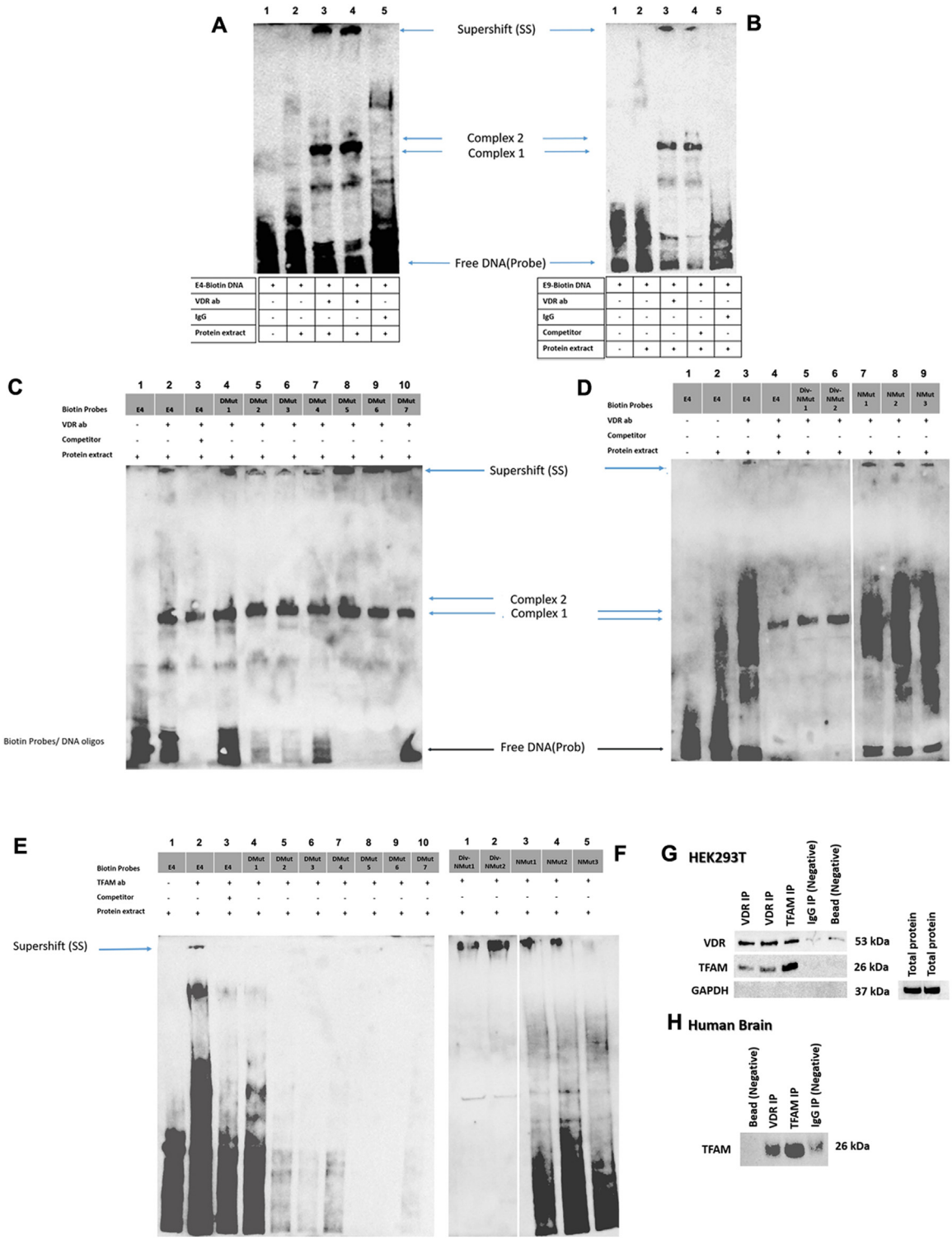

Fig. 5. (A–B) EMSA assay with wild-type sequences for VDR binding. (A) EMSA assay for testing the binding of VDR to the wild type (WT) E4 sequence. EMSA was performed with 100 fmol (lane 3) or 50 fmol (lane 4) of biotinylated double-stranded oligonucleotides and 13 μg total protein extract of VDR overexpressed, and 10^{-8} M 1,25OH2D3 treated HEK293T cells. 3.5 μg anti-VDR antibody was added to the EMSA reaction mixture. Normal IgG was used as a negative control. As a result, several complexes were seen in the groups incubated with anti-VDR antibody. Complex 1 has always shown a strong, bold band profile, while Complex 2 has a relatively weak band. (B) Biotin-labeled WT E9 DNA sequence of the mtDNA D-loop region was used to test VDR binding. EMSA was performed with 100 fmol of biotinylated double-stranded oligonucleotides, and 13 μg total protein extract of VDR overexpressed and 10^{-8} M 1,25OH2D3 treated HEK293T cells. For the supershift assays, a 3.5 μg anti-VDR antibody was added to the mixture. For the competition assay, an 800-fold molar excess of unlabeled oligonucleotides was added to the binding mixture. The supershift bands and bindshift bands are indicated by arrows. Similar to the results of E4, E9 showed several complexes when an anti-VDR antibody was presented. Sequence information was given in Table 1. (C) EMSA assay with mutant oligomers (deletion mutants-DMuts). EMSA assay results of seven deletion mutants (DMut 1–7) of E4 and WT E4 oligo. To determine whether the VDR binds to the E4 region in a sequence-specific manner, seven E4-DMuts were designed. Total cellular extracts of VDR overexpressing and 10^{-8} M 1,25OH2D3 treated HEK293T cells were used. Lane 1 shows the biotinylated WT-E4 probe incubated with the extract. Lane 2 shows the biotinylated WT-E4 probe incubated with the cell extract and anti-VDR antibody. Lane

chosen and split into nine different sites (amplified by E1-E9 primers) according to alignment results (Supplementary Material 1) to get smaller DNA fragments for EMSA assay. The region amplified by D1 primers was split into smaller regions that were amplified by E1-E4 primers; similarly, the D2 region was split as E5-E6, the D3 region was split as E7-E8, and E9 primer was created to narrow down the D4 region. The ChIP experiment was repeated with these new primers (E1-E9) to understand the specificity of VDR binding. According to the new ChIP-qPCR results, the fold enrichments over IgG for all sites amplified by E1-E9 primers were higher than 3. Still, the mtDNA sequence amplified with E4 primers had higher fold enrichment than other regions. The E9 has the lowest one, but the fold enrichment was still higher than 3 (data not shown). As a result, the region amplified by E4 primers (the highest amplified) was determined as a candidate region for the VDR binding site. E9 site (the lowest amplified->3) was used as a control in the EMSA assay. The regions amplified by E4 and E9 primers were synthesized as sense and anti-sense sequences.

3.5.3. Technical confirmation of the methodology of EMSA for known VDRE

Before further EMSA experiments, we wanted to test the methodology of EMSA assay for VDREs and the binding capacity of anti-VDR antibody in EMSA. So, first, we used a known nuclear DNA binding site for VDR, VDRE for the 24-hydroxylase (24OHase) gene [63,64], and we showed the binding of VDR to the target sequence in EMSA assay (Supplementary Fig. 7).

3.5.4. EMSA for selected mtDNA fragments

After verifying the methodology, the EMSA was performed with E4 or E9 regions with anti-VDR antibody or IgG (negative control). Both regions gave specific supershift bands, and E4 or E9 EMSA with IgG confirmed the specificity of the bands (Figure 5A and B). EMSA assays were continued with the E4 mtDNA region. After we got supershift bands, we did further EMSA assays with different mutant oligonucleotides to identify a DNA sequence specific to VDR. E4 mtDNA region was re-analyzed for known vitamin D response elements (VDREs) and similar sequences in the D-loop by alignment tools. We identified four sequences (WT E4 sequence marked with different colors for these sites in Table 1).

3.5.5. Confirming novel VDRE in selected mtDNA fragments with mutated sequences in EMSA

After the first EMSAs and alignment analysis, we used two strategies to identify specific VDR binding sites. EMSA assay was repeated with the following mutants. The first seven different "Deletion Mutants," named E4-DMut1-7, were created by the deletion of specific sites (Table 1). The supershift bands E4- DMut2, 3, and 4 were very weak but still there, and E4-DMut 6 was still giving band even though it did not include all of these regions (Fig. 5C). Simultaneously, three different mutant sequences were created in E4 possible binding regions and named as E4-Nucleotide Exchange mutant (E4-NMut) 1–3 (Table 1). The EMSA results of E4-NMuts for VDR binding were unsatisfactory (Fig. 5D). According to DMut and NMut results, we thought there might be several binding regions for VDR, or the binding of VDR to mtDNA was not specific. We looked over the mutations we created in NMuts and realized that we mistakenly created a specific VDRE (for osteocalcin and MIS) in the blue region. But these NMuts were still useful, giving us important information about TFAM binding sequence in the E4 region. Following the DMut and NMut EMSA results, we thought that VDR binding might be affected by some conformational changes in the E4 region. Therefore, with data from TFAM-NMut3 EMSA and Co-IP experiments (the binding sites of VDR and TFAM may also be in close proximity if they have interaction), we created the new mutants in half-site of E4, approximately dividing E4 into two, which includes the TFAM binding site (Divided Sequence Nucleotide Exchange mutant—E4-DivNMut 1 and 2) (Table 1) and EMSA was repeated for VDR. Regarding the EMSA result (Fig. 5D), we found possible specific sites for VDR binding "**CAAGCA**agt**ACAGCA**" **(mtDNA coordinates nt 16,202–16,216)**. VDR lost the binding ability with the mutation only in "**CAAGCA**" (DivNMut 2). In these DivNMuts we did not see Complex 2. The Complex 1 band intensity decreased with the "**CAAGCA**agt**ACAGCA**" mutant (DivNmut 1). This area consisted of the knowledge that **VDRE** typically consists of two conserved hexameric half-sites separated by a three-nucleotide spacer. So, these sites were aligned in D-loop regions that were amplified by D1-D9 primers. We cannot find the same hexameric half-sites separated by a three-nucleotide spacer. But we found similar hexameric repeats in all regions and analyzed them with STAMP. STAMP gave the "**MMHKCA**" motif as a consensus sequence (Fig. 1).

3.5.6. Defining novel binding site for TFAM with EMSA

ChIP results showed that TFAM could bind to the region amplified by the D1 primer (the E4 region is in the D1 region). We also repeated the EMSA assay with the E4 region and anti-TFAM antibody, and the supershift band confirmed the TFAM binding capacity to the E4 region (Fig.5E). EMSA with IgG (as a negative control) or anti-TFAM antibody results showed that VDR could form another specific complex independent from the supershift band (Fig. 5A and E). EMSA assay was repeated with anti-TFAM antibody and DMuts, NMuts, or DivNMuts (Fig. 5E and F). Interestingly supershift band of TFAM was lost only in DMuts and NMut3. When we compared all mutants, the NMut3 mutant had specific

3 shows the competition assay that was performed with the addition of unlabeled competitor WT E4 DNA. Lines 4–10 show DMuts. Complex 1 was presented in all of the anti-VDR antibody-treated groups and seemed not affected by the deletions. Though, Complex 2 was affected by deletions. Supershift bands were also showed different signal intensity depending on the mutants: the signal was weakened in DMut2, DMut3, DMut4. Sequence information was given in Table 1. (D) EMSA assay with mutant oligomers (NMuts and DivNMuts). EMSA supershifts of WT-E4 and divided nucleotide exchange (DivNMut 1 and 2) or nucleotide exchange (NMuts 1–3) E4 mutants. Lane 1 shows free wt-E4 DNA probe only. Lane 2 shows the interaction of wt-E4, and total cell extracts from VDR overexpressing 10^{-8} M 1,25OH2D3 treated HEK293T cells. Lane 3 shows the VDR-supershifted band. Lane 4 shows the competition assay. EMSA supershift assay result was showed no supershifted bands of Div-NM1 and Div-NM2 sequences (Lanes 4, 5). Otherwise, supershifted bands were detected for NMut1, NMut2, and NMut3 (Lanes 7–9). Additionally, Complex 2 was affected in both DivNmut oligos. (E and F) EMSA assay for TFAM. The interaction of TFAM with wild type-E4 and mutated E4 oligos was determined by EMSA supershift. For the supershift assays, a 3.5 μg TFAM antibody was added to the EMSA reaction mix after the addition of WT-E4 DNA probe (Lane 2). For competition assays, an 800-fold molar excess of unlabeled WT-E4 oligonucleotides was used (Lane3). EMSA was performed with seven biotin-labeled DMut 1–7 probes to determine whether the TFAM binds to the E4 oligo in a sequence-specific manner. No supershift bands were detected of TFAM with DMut oligos. These DMuts did not carry a few nucleotides at the 3′-end, which we later identified as the TFAM binding site. EMSA of other mutants showed supershifted bands for DivNMut1, DivNMut2, NMut1, and NMut2 except for NMut3. Arrows indicate the supershift bands. Sequence information of oligos was given in Table 1. (G and H) VDR and TFAM Co-IP: (G) VDR or TFAM proteins immunoprecipitated in HEK293T cell lysates. Anti-VDR antibody labeling indicated VDR is present in pull-down samples of two independent VDR IPs and TFAM IP but not in IgG IP or bead treated samples. Anti-TFAM antibody labeling showed TFAM is present in pull-down samples of VDR IPs and TFAM IP but not in IgG IP or bead treated samples. Anti-GAPDH antibody labeling indicated GAPDH is not present in any pull-down samples but present in total protein extracts. (H) VDR or TFAM proteins immunoprecipitated in human brain lysates. Anti-TFAM antibody labeling indicated TFAM presence both in VDR- or TFAM-IP groups. VDR IP: Sample immunoprecipitated with anti-VDR antibody, TFAM IP: Sample immunoprecipitated with anti-TFAM antibody, IgG IP: Sample immunoprecipitated with anti-IgG antibody (negative control), Bead: Sample immunoprecipitated with empty beads without any antibody, Total protein: Since GAPDH was not present in any IPs, it was also labeled in total protein extracts.

nucleotide changes in the "TCAACC" (nt 16,218–16,223) sequence, which is similar to one of the known TFAM binding sites in LSP [64,65]. Furthermore, the DivNMuts did not carry the last "C" nucleotide, and the TFAM binding continued in these mutants. Additionally, DMuts did not carry the last "CC" nucleotides, and we cannot see supershift with anti-TFAM antibody. So similar to LSP, it seems that for TFAM binding, the last "C" is necessary for the "TCAADC" sequence. This data indicated an additional binding site for TFAM independent from Site Y, Site X, or LSP. Moreover, this site is in close proximity to the possible VDRE in mtDNA that we identified: **"CAAGCA**agtACAGCAa**TCAAC"** (nt 16,202–16,222)**.** Similar sequences were also found in known TFAM binding sites: Between Site Y and Site X **"ACATCA" (nt 277–282)** and in LSP **"CAGTCA" (nt 427–433)**.

3.6. Co-immunoprecipitation (Co-IP) results

Our ChIP results and BrdU labeling showed that VDR could bind to mtDNA. However, we also took into account that VDR may bind mtDNA both directly or indirectly through TFAM. The possible interaction between VDR and TFAM was examined by WB following Co-IP experiments, in which used specific antibodies targeting VDR or TFAM from HEK293T cell or human brain lysates. IP samples that we used VDR and TFAM antibodies are named VDR-IP and TFAM-IP, respectively. Bead-only and non-target IgG IP samples were used as negative controls. Besides, HEK total protein samples were used as a positive control.

For the WB analysis of IP samples, we first targeted VDR on the membrane. VDR-IP and HEK total protein samples showed positive signals at approximately 50 kDa compared to negative controls, as expected. In addition to this, we also determined a positive signal on TFAM-IP samples after immunoblotting with the anti-VDR antibody. These results showed that TFAM precipitates with VDR. To confirm VDR immunoblotting results, we then targeted TFAM on the membrane that has the same samples (Fig. 5G). TFAM-IP and HEK total proteins have a strong TFAM signal at approximately 23 kDa, contrary to negative control IP samples. Confirming our VDR immunolabeling results, we detected positive signals for VDR-IP samples after immunoblotting with anti-TFAM antibody compared to negative control IP samples. VDR- and TFAM-IP, followed by TFAM immunolabeling of human brain lysates, verified the interaction between the two proteins (Fig. 5H). According to VDR- and TFAM-IP results, we, for the first time, showed that TFAM precipitates with VDR.

4. Discussion

In the present study, we aimed to show the ability of VDR in the direct regulation of mtDNA transcription. We focused on energy-demanded cells, particularly neuronal cells. We showed that vitamin D3/VDR affects the expression of mtDNA encoded (OXPHOS) subunits. Furthermore, we observed the co-localization of VDR with mitochondria and the mtDNA. mtDNA-ChIP assays and further EMSA analysis indicated that VDR was able to bind to the mtDNA D-loop site in several locations. We also reported the possible interaction between VDR and TFAM. To the best of our knowledge, this is the first report that shows VDR is able to regulate mtDNA transcription and interact with TFAM.

We previously showed the effect of vitamin D3 or VDR on the gene expression of neurodegeneration-related genes [10,12,15-20,23,24]. It was not surprising, given that VDR is a transcription factor and can bind to nuclear DNA. However, we know that VDR localized in mitochondria [34], an organelle with extranuclear DNA, the mitochondrial DNA (mtDNA). Vitamin D's role in mitochondrial biogenesis and functions has been shown in various studies, including different cell types. However, these studies linked their findings to the extramitochondrial biochemical events of vitamin D [37–40]. Nevertheless, the question remained unanswered: may some effects of vitamin D on mitochondria be related to its role in the direct regulation of the mitochondrial genome?

First, we examined our proposition in primary cortical neuron culture by administering two doses of 1,25OHD in two separate treatment periods. Following that, mRNA levels of 13 mtDNA encoding OXPHOS subunits were determined. The mRNA expressions of most of the subunits were changed by 1,25OHD treatment. Furthermore, the ATP levels were increased in response to 1,25OHD. Consistently in other cell types, for example, in rat granulosa cells, it was shown that 1,25OHD treatment increased MT-CO1 protein expression and induced increases in ATP levels [39]. Ryan et al. reported that 1,25OHD changes skeletal muscle mitochondrial oxygen consumption rate (OCR), dynamics, enzyme function, and expression of nuclear genes encoding mitochondrial proteins. Although Ryan et al. could not detect VDR in mitochondria, they showed its presence in the cytoplasm of human skeletal muscle cells. They suggested that the effects of 1,25OHD on OCR depend on extramitochondrial biochemical events [37].

After 1,25OHD treatment results, the effect of vitamin D3 on mtDNA encoding OXPHOS subunits in cortical neurons was obvious. The question was whether this effect was due to VDR or not. So, we silenced VDR in primary cortical neurons. VDR silencing showed us that VDR itself could significantly influence mtDNA mRNA expression, and these changes were mostly similar to the changes in the amount of protein. In a different cell type, C2C12 myoblasts and myotubes, a requirement for the VDR to maintain optimal mitochondrial respiration has been reported. The investigators suggested that the observed reductions in mitochondrial function after VDR silencing resulted from reduced ATP. In contrast, they also suggested that markers of mitochondrial protein content were unchanged [66]. It seems that VDR is essential for mitochondrial function, but its effect on mtDNA expression depends on cell type, which is not surprising according to ENCODE results [8].

In the present study, VDR was overexpressed in cortical neurons, and VDR overexpressing neurons were treated with 1,25OHD. *MT-ND1, MT-ND3, MT-ND4, MT-ND4L, MT-ND5, MTCO1, MT-CO2,* and *MT-ATP8* mRNA levels were altered in VDR overexpressing and/or 1,25OHD treated VDR overexpressing groups. Only MT-ND6 expression was not related to VDR but changed by 1,25OHD treatment. The studies showed that vitamin D and/or VDR have different effects on cellular mechanisms, which depend on cell type. Thus, we wanted to test the effect of vitamin D and VDR on mtDNA expression in other cell types, namely PC12, a neuronal cell line. We choose this cell for several reasons. First, it originated from rats, like primary cortical neurons. Second, it can be differentiated to neuron-like cells by NGF. The third and most important reason was its response to vitamin D differs greatly from other cell types. Vitamin D via VDR has been shown to promote differentiation and inhibit the proliferation of various normal and malignant cell types [67]. However, vitamin D application seemed to have a different effect on PC12 cells. Vitamin D displayed no effect on PC12 cell growth, although it was capable of inhibiting the melatonin-induced suppression of PC12 cell growth [62]. We thought that the different responses of vitamin D in PC12 might depend on the VDR expression level. Thus, before the experiments, we compared VDR mRNA expression levels of primary cortical neurons and PC12 cells. We found that PC12 cells expressed dramatically low levels of VDR than primary cortical neurons. Because of that, we did not silence VDR in PC12. Instead of that, we choose to overexpress it. Although there are some similarities, most results were different in PC12 cells, as we expected. The results showed us that the action

of vitamin D varies with the cell type. However, it ultimately alters the expression of genes encoded in mtDNA for cultured primary neurons or PC12 cells.

Given their role in mitochondrial quality control, the effect of vitamin D3 on the mRNA expression levels of nuclear DNA encoding PTEN-induced putative kinase 1 (PINK1) and a ubiquitin E3 ligase PARKIN were also investigated [68,69]. Both of them, especially PARKIN mRNA levels, were changed in response to 1,25OHD and/or VDR silencing/overexpressing. This remarkable change of PARKIN mRNA with vitamin D3/VDR might be related to the ubiquitination of the nuclear receptors' mechanism [70]. However, this relationship could also affect the regulation of mitochondrial quality control mechanisms. Interestingly supporting results come from human keratinocytes. Limited energy availability in human keratinocytes after exposure to UV was reported to increase by 1,25OHD, which stimulated autophagy and regulated PINK1/Parkin mediated mitophagy [71].

Reviewing all mRNA expression results obtained from primary cortical neurons (Table 2), we see that the mRNA expressions of the *MT-ND4L, MT-ND5, MT-CO1*, and *MT-CO2* genes increase in the presence of vitamin D3 and VDR and decrease in the absence of VDR. In contrast, *MT-ND2, MT-CYB*, and *MT-CO3* do not change in the presence of vitamin D3 and VDR but decrease only in the absence of VDR. Different vitamin D compounds like CYP11A1-derived including 20(OH)D3 and 20,23(OH)2D3 or tachysterol3 hydroxyderivatives, also can bind to VDR [3-5,72,73] and this might explain why we only saw VDR silencing effect for some mRNAs but could not see the effect of 1,25OHD on same mRNAs in our experimental setup. However, the situation gets more complicated for other mRNAs, and the presence or absence of VDR or 1.25OHD creates a complex picture. Explanation of this complex results might be the possible interaction behavior of 1,25OHD or vitamin D compounds with other receptors like Aryl hydrocarbon receptor (AhR), liver X receptors (LXRs), or the retinoic acid-related orphan receptors α–γ (RORα–γ) [72–76]. Although the results were complicated, we still found that our main target, the VDR, changed the expression of the genes encoded from mtDNA.

However, it was still unclear if VDR was in the neurons' mitochondria. There are controversial results about the localization of VDR in mitochondria, Silvagno et al. showed its presence in several cell types [34,35], but Ryan et al. reported that VDR did not localize in the mitochondria of skeletal muscle cells [37]. Mitotracker staining and VDR immunolabeling in our study revealed the localization of VDR in mitochondria of primary cortical neurons for the first time. At this point, we wanted to use another type of cell that originated from humans, SH-SY5Y. Similarly, the presence of VDR in mitochondria was also confirmed in SH-SY5Y cells. Following that, the mtDNA of these cells was labeled by BrdU and double-labeled by VDR, and possible mtDNA-VDR interaction was reported for the first time in rat primary cortical neurons and human SH-SY5Y cells.

Furthermore, we confirmed the binding ability of VDR on the D-loop of mtDNA in four different cell types and the human brain tissues of three individuals by mitochondrial ChIP analysis. Human kidney-derived cell line HEK-293T, which is known to express VDR and several of its genes are known to be regulated by 1,25OHD, was chosen. Additionally, this cell type was previously used for nuclear ChIP analysis of VDR [77,78]. Human SH-SY5Y cells were chosen because of their neuron-like character. ChIP analysis was performed only once in primary neurons and was not repeated because it requires an excessive number of cells. An unmodified cell, the PBMC pool of healthy individuals was selected for mitochondrial ChIP analysis. ChIP was repeated with the human brain tissue samples to confirm and conclude our results. In all sample types, the binding ability of VDR to mtDNA was different from each other. In HEK293T cells, its binding affinity was very similar to TFAM and indicated several binding sites, though, in PBMCs, it could bind only one region on the D-loop. Although the binding pattern differed from the other two cell types, SH-SY5Y cells' data also indicated several binding sites for VDR on mtDNA. Nevertheless, interestingly primary cortical neurons of rats and, most notably, in human brain tissues of three different individuals showed very strong VDR binding affinity. In all three human brain samples, VDR binding affinity was greater than TFAM. Furthermore, ChIP qRT-PCR results in HEK293T cells with 18 primers which cover other parts of mtDNA, showed that VDR binding affinity might not be limited within the D-loop region. But this finding should be repeated in other cell types.

It was suggested that TFAM binds mtDNA approximately every 35 base pairs as a dimer, regardless of sequence, suggested to be principal contributor to mtDNA organization and to regulate mtDNA copy number [79]. Given that our ChIP results indicated similar binding patterns for both VDR and TFAM not only on the D-loop region but also on the mtDNA gene coding region and other mtDNA regions, we investigated a possible direct relationship between TFAM and VDR. Our IP results revealed that VDR interacts with TFAM in HEK-293T cells and human brain tissue for the first time. String data showed that peroxisome proliferator-activated receptor γ coactivator-1α (PGC-1α) is the only mutual protein between VDR and TFAM. On the one hand, it was shown that PGC-1α re-localizes into nuclear and mitochondrial compartments, where it functions as a transcriptional co-activator for both nuclear and mtDNA transcription factors. It is in a complex with TFAM at mtDNA D-loop in mitochondria in response to acute energy demands in mice [80]. On the other hand, Savkur et al. reported that PGC-1α serves as a co-activator for VDR in HEK293 cells [81]. Thus, PGC-1α might also serve as an additional protein for the relationship between TFAM and VDR. Furthermore, the co-existence of VDR with TFAM, especially outside of known binding sites, might indicate the possibility of VDR participation in mtDNA organization in specific cell types. The EMSA results allow us to suggest strongly that TFAM and VDR can bind to sequences in close proximity. Further studies should be done to identify the interaction pattern of VDR with mtDNA or TFAM.

Dr. Eyles recently reviewed the effect of developmental or adult vitamin D deficiency on the brain and concluded the increased risk of vitamin D deficiency in neurodevelopmental disorders and certain adult degenerative conditions [82]. Vitamin D deficiency seems to be related to brain energy metabolism according to transcriptome and proteome results [83]. Proteomic analysis showed that developmental vitamin D deficiency affected six nuclear-encoded mitochondrial proteins in rat nucleus accumbens [84]. Keisala et al. showed that VDR knockout mice showed several aging-related phenotypes and suggested that the ablation of VDR promotes premature aging [85]. In the present study, we demonstrated that VDR could bind to mtDNA and regulate the expression of OXPHOS subunits. We know the tight relationship between mitochondria and aging [86]. VDR might be a strong cofounder of this relationship.

From an evolutionary perspective, it is suggested that cartilaginous (non-calcified) jawless fishes possess an ancestral form of VDR, which is involved in xenobiotic detoxification but not in calcification [87]. The xenobiotic detoxification pathway is also suggested to interconnect with many lifespan extension mechanisms. These mechanisms include the ones related to mitochondrial dysfunction. Besides, mitochondrial dysfunction is also associated with the expression of different mitochondrial respiratory chain subunits [88]. Our results showed that VDR is a possible TF for mtDNA and works with TFAM, but this function of VDR is cell-type specific. It might also be speculated from the information about VDR's

first known role, which is not related to calcification, but mitochondrial events, the mtDNA regulation, is one of the main functions of VDR in specific or energy-demanded cells. On the other hand, findings in UV-exposured human keratinocytes indicate that it may also be important for mitochondrial function in cells with limited capacity to produce energy [71,75].

In conclusion, the present study showed that vitamin D3 and/or VDR are essential for proper mitochondrial function in neuronal cells, even in the human brain. This novel information and our earlier studies, which are related to vitamin D and VDR in neurodegeneration, encourage us to speculate that the imbalance of this secosteroid hormone or its receptor has crucial roles in the development and progress of mitochondrial dysfunction related diseases like neurodegenerative disorders. Furthermore, this new role of the VDR could apply to any cell in which the VDR runs.

Authors' contributions

Conceptualization: D.G.A., E.D; Data Curation: D.G.A., M.A., B.Ş., C.İ., U.Y.K., E.K., I.L.A., Z.Y., T.Ç., A.M.K., M.U., E.D; Formal Analysis: D.G.A., M.A., Z.Y., E.D; Funding Acquisition: D.G.A; Investigation: D.G.A., M.A., Z.Y., T.Ç., E.D; Methodology: D.G.A., M.A., Z.Y., T.Ç., E.D; Project Administration: D.G.A., E.D; Resources: D.G.A., E.D; Supervision: D.G.A., E.D; Validation: D.G.A., E.D; Writing – Original Draft Preparation: D.G.A., M.A., B.Ş., C.İ., E.K., Z.Y., T.Ç., E.D; Writing – Review & Editing: D.G.A., C.A., E.D. All authors read and approved the final manuscript.

Acknowledgments

We would like to thank Professor Slyvia Christakos of Rutgers New Jersey Medical School and her team for their generous help, sharing their knowledge and technical expertise on nuclear ChIP analysis.

Declaration of competing interests

Duygu Gezen-Ak, Merve Alaylıoğlu, Zuhal Yurttaş, Tugay Çamoğlu, Büşra Şengül, Cihan İşler, Ümit Yaşar Kına, Ebru Keskin, İrem Lütfiye Atasoy, Ali Metin Kafardar, Mustafa Uzan, Cedric Annweiler, Erdinç Dursun declare that they have no conflict of interest.

Funding

The study is supported by the Scientific and Technological Research Council of Turkey-TUBITAK (Project No. 115S438) and by Research Fund of Istanbul University-Cerrahpasa (Project No: DKEP-35917). The funders had no role in study design, data collection and analysis, decision to publish, or preparation of the manuscript.

Ethical approval

The Animal Welfare and Ethics Committee of Istanbul University approved the study with the number 26.07.2012/101. All procedures were done following both the guide of the Istanbul University and National Research Council's manual for the care and use of laboratory animals. Participants in the present study were treated according to the ethical principles for medical research involving human participants described in the World Medical Association's Declaration of Helsinki, and the study was approved by the Ethics Committee of Istanbul University-Cerrahpasa. Signed informed consent was obtained from all study participants.

Availability of data and materials

All data generated or analyzed during this study are included in this published article and its supplementary information files.

Supplementary materials

Supplementary material associated with this article can be found, in the online version, at doi:10.1016/j.jnutbio.2023.109322.

References

[1] Christakos S, Ajibade DV, Dhawan P, Fechner AJ, Mady LJ, et al. Vitamin D: metabolism. Endocrinol Metab Clin North Am 2010;39(2):243–53 table of contents.
[2] Slominski AT, Kim TK, Shehabi HZ, Semak I, Tang EK, Nguyen MN, et al. In vivo evidence for a novel pathway of vitamin D(3) metabolism initiated by P450scc and modified by CYP27B1. FASEB J 2012;26(9):3901–15.
[3] Slominski AT, Kim TK, Shehabi HZ, Tang EK, Benson HA, Semak I, et al. In vivo production of novel vitamin D2 hydroxy-derivatives by human placentas, epidermal keratinocytes, Caco-2 colon cells and the adrenal gland. Mol Cell Endocrinol 2014;383(1-2):181–92.
[4] Slominski AT, Li W, Kim TK, Semak I, Wang J, Zjawiony JK, et al. Novel activities of CYP11A1 and their potential physiological significance. J Steroid Biochem Mol Biol 2015;151:25–37.
[5] Slominski AT, Kim TK, Li W, Postlethwaite A, Tieu EW, Tang EKY, et al. Detection of novel CYP11A1-derived secosteroids in the human epidermis and serum and pig adrenal gland. Sci Rep 2015;5:14875.
[6] Issa L, Leong GM, Eisman JA. Molecular mechanism of vitamin D receptor action. Inflamm Res 1997;47:451–75.
[7] Freedman LP, Arce V, Perez Fernandez R. DNA sequences that act as high affinity targets for the vitamin D3 receptor in the absence of the retinoid X receptor. Mol Endocrinol 1994;8(3):265–73.
[8] Carlberg C. Genome-wide (over)view on the actions of vitamin D. Front Physiol 2014;5:167.
[9] Annweiler C, Dursun E, Feron F, Gezen-Ak D, Kalueff AV, Littlejohns T, et al. *'Vitamin D and cognition in older adults': updated international recommendations.* J Intern Med 2015;277(1):45–57.
[10] Dursun E, Gezen-Ak D, Yilmazer S. The influence of vitamin D treatment on the inducible nitric oxide synthase (INOS) expression in primary hippocampal neurons. Noro Psikiyatr Ars 2014;51(2):163–8.
[11] Dursun E, Alaylioglu M, Bilgic B, Hanagasi H, Lohmann E, Atasoy IL, et al. Vitamin D deficiency might pose a greater risk for ApoEvarepsilon4 non-carrier Alzheimer's disease patients. Neurol Sci 2016;37(10):1633–43.
[12] Dursun E, Candas E, Yilmazer S, Gezen-Ak D, et al. Amyloid beta 1-42 alters the expression of miRNAs in cortical neurons. J Mol Neurosci 2019;67(2):181–92.
[13] Dursun E, Gezen-Ak D. Vitamin D receptor is present on the neuronal plasma membrane and is co-localized with amyloid precursor protein, ADAM10 or Nicastrin. PLoS One 2017;12(11):e0188605.
[14] Dursun E, Gezen-Ak D. Vitamin D basis of Alzheimer's disease: from genetics to biomarkers. Hormones (Athens) 2018.
[15] Dursun E, Gezen-Ak D, Yilmazer S. A novel perspective for Alzheimer's disease: vitamin D receptor suppression by amyloid-beta and preventing the amyloid–beta induced alterations by vitamin D in cortical neurons. J Alzheimers Dis 2011;23(2):207–19.
[16] Dursun E, Gezen-Ak D, Yilmazer S. A new mechanism for amyloid-beta induction of iNOS: vitamin D-VDR pathway disruption. J Alzheimers Dis 2013;36(3):459–74.
[17] Dursun E, Gezen-Ak D, Yilmazer S. Beta amyloid suppresses the expression of the vitamin d receptor gene and induces the expression of the vitamin d catabolic enzyme gene in hippocampal neurons. Dement Geriatr Cogn Disord 2013;36(1-2):76–86.
[18] Gezen-Ak D, Dursun E, Yilmazer S. The effects of vitamin D receptor silencing on the expression of LVSCC-A1C and LVSCC-A1D and the release of NGF in cortical neurons. PLoS One 2011;6(3):e17553.
[19] Gezen-Ak D, Dursun E, Yilmazer S. Vitamin D inquiry in hippocampal neurons: consequences of vitamin D-VDR pathway disruption on calcium channel and the vitamin D requirement. Neurol Sci 2013;34(8):1453–8.
[20] Gezen-Ak D, Dursun E, Yilmazer S. The effect of vitamin D treatement on nevre growth factor release (NGF) in hippocampal neurons. Noro Psikiyatr Ars 2014;51(2):157–62 Jun. doi:10.4274/npa.y7076.
[21] Gezen-Ak D, Alaylioglu M, Genc G, Gunduz A, Candas E, Bilgic B, et al. GC and VDR SNPs and vitamin D levels in Parkinson's disease: the relevance to clinical features. Neuromol Med 2017;19(1):24–40.
[22] Gezen-Ak D, Alaylioglu M, Genc G, Sengul B, Keskin E, Sordu P, et al. Altered transcriptional profile of mitochondrial DNA-encoded OXPHOS subunits, mitochondria quality control genes, and intracellular ATP levels in blood samples of patients with Parkinson's disease. J Alzheimers Dis 2020;74(1):287–307.

[23] Gezen-Ak D, Atasoy IL, Candas E, Alaylioglu M, Dursun E, et al. The transcriptional regulatory properties of amyloid beta 1-42 may include regulation of genes related to neurodegeneration. Neuromolecular Med 2018;20(3):363–75.
[24] Gezen-Ak D, Atasoy IL, Candas E, Alaylioglu M, Yilmazer S, Dursun E, et al. Vitamin D receptor regulates amyloid beta 1-42 production with protein disulfide isomerase A3. ACS Chem Neurosci 2017;8(10):2335–46.
[25] Gezen-Ak D, Dursun E. Molecular basis of vitamin D action in neurodegeneration: the story of a team perspective. Hormones (Athens) 2019;18(1):17–21 Mar. doi:10.1007/s42000-018-0087-4.
[26] Gezen-Ak D, Dursun E, Bilgic B, Hanagasi H, Ertan T, Gurvit H, et al. Vitamin D receptor gene haplotype is associated with late-onset Alzheimer's disease. Tohoku J Exp Med 2012;228(3):189–96.
[27] Gezen-Ak D, Dursun E, Ertan T, Hanagasi H, Gurvit H, Emre M, et al. Association between vitamin D receptor gene polymorphism and Alzheimer's disease. Tohoku J Exp Med 2007;212(3):275–82.
[28] Gezen-Ak D, Yilmazer S, Dursun E. Why vitamin D in Alzheimer's disease? The hypothesis. J Alzheimers Dis 2014;40(2):257–69.
[29] Yan MH, Wang X, Zhu X. Mitochondrial defects and oxidative stress in Alzheimer disease and Parkinson disease. Free Radic Biol Med 2013;62:90–101.
[30] Pinto M, Moraes CT. Mitochondrial genome changes and neurodegenerative diseases. Biochim Biophys Acta 2014;1842(8):1198–207.
[31] Gavrilova-Jordan LP, Price TM. Actions of steroids in mitochondria. Semin Reprod Med 2007;25(3):154–64.
[32] Klinge CM. Estrogenic control of mitochondrial function. Redox Biol 2020;31:101435.
[33] Psarra AM, Sekeris CE. Glucocorticoids induce mitochondrial gene transcription in HepG2 cells: role of the mitochondrial glucocorticoid receptor. Biochim Biophys Acta 2011;1813(10):1814–21.
[34] Silvagno F, De Vivo E, Attanasio A, Gallo V, Mazzucco G, Pescarmona G, et al. Mitochondrial localization of vitamin D receptor in human platelets and differentiated megakaryocytes. PLoS One 2010;5(1):e8670.
[35] Silvagno F, Consiglio M, Foglizzo V, Destefanis M, Pescarmona G, et al. Mitochondrial translocation of vitamin D receptor is mediated by the permeability transition pore in human keratinocyte cell line. PLoS One 2013;8(1):e54716.
[36] Ricca C, Aillon A, Bergandi L, Alotto D, Castagnoli C, Silvagno F. Vitamin D Receptor Is Necessary for Mitochondrial Function and Cell Health. Int J Mol Sci 2018;19(6):1672 Jun.
[37] Ryan ZC, Craig TA, Folmes CD, Wang X, Lanza IR, Schaible NS, et al. 1alpha,25-dihydroxyvitamin D3 regulates mitochondrial oxygen consumption and dynamics in human skeletal muscle cells. J Biol Chem 2016;291(3):1514–28.
[38] Dzik KP, Kaczor JJ. Mechanisms of vitamin D on skeletal muscle function: oxidative stress, energy metabolism and anabolic state. Eur J Appl Physiol 2019;119(4):825–39.
[39] Lee CT, Wang JY, Chou KY, Hsu MI, et al. 1,25-Dihydroxyvitamin D3 modulates the effects of sublethal BPA on mitochondrial function via activating PI3K-Akt pathway and 17beta-estradiol secretion in rat granulosa cells. J Steroid Biochem Mol Biol 2019;185:200–11.
[40] Mocayar Maron FJ, Ferder L, Reiter RJ, Manucha W, et al. Daily and seasonal mitochondrial protection: unraveling common possible mechanisms involving vitamin D and melatonin. J Steroid Biochem Mol Biol 2020;199:105595.
[41] Avalle L, Poli V. Nucleus, mitochondrion, or reticulum? STAT3 a La Carte. Int J Mol Sci 2018;19(9):2820. doi:10.3390/ijms19092820.
[42] Chatterjee A, Seyfferth J, Lucci J, Gilsbach R, Preissl S, Bottinger L, et al. MOF acetyl transferase regulates transcription and respiration in mitochondria. Cell 2016;167(3):722 38.e23.
[43] Johnson RF, Witzel II, Perkins ND. p53-dependent regulation of mitochondrial energy production by the RelA subunit of NF-kappaB. Cancer Res 2011;71(16):5588–97.
[44] Lambertini E, Penolazzi L, Morganti C, Lisignoli G, Zini N, Angelozzi M, et al. Osteogenic differentiation of human MSCs: specific occupancy of the mitochondrial DNA by NFATc1 transcription factor. Int J Biochem Cell Biol 2015;64:212–19.
[45] Blumberg A, Sri Sailaja B, Kundaje A, Levin L, Dadon S, Shmorak S, et al. Transcription factors bind negatively selected sites within human mtDNA genes. Genome Biol Evol 2014;6(10):2634–46.
[46] Macias E, Rao D, Carbajal S, Kiguchi K, DiGiovanni J, et al. Stat3 binds to mtDNA and regulates mitochondrial gene expression in keratinocytes. J Invest Dermatol 2014;134(7):1971–80.
[47] Leigh-Brown S, Enriquez JA, Odom DT. Nuclear transcription factors in mammalian mitochondria. Genome Biol 2010;11(7):215.
[48] Morrish F, Buroker NE, Ge M, Ning XH, Lopez-Guisa J, Hockenbery D, et al. Thyroid hormone receptor isoforms localize to cardiac mitochondrial matrix with potential for binding to receptor elements on mtDNA. Mitochondrion 2006;6(3):143–8.
[49] Consiglio M, Destefanis M, Morena D, Foglizzo V, Forneris M, Pescarmona G, et al. The vitamin D receptor inhibits the respiratory chain, contributing to the metabolic switch that is essential for cancer cell proliferation. PLoS One 2014;9(12):e115816.
[50] . Guide for the care and use of laboratory animals. Washington, DC.: National Academies Press; 2011. p. 220.
[51] Shaw G, Morse S, Ararat M, Graham FL, et al. Preferential transformation of human neuronal cells by human adenoviruses and the origin of HEK 293 cells. FASEB J 2002;16(8):869–71.
[52] Davis AF, Clayton DA. In situ localization of mitochondrial DNA replication in intact mammalian cells. J Cell Biol 1996;135(4):883–93.
[53] Park CB, Asin-Cayuela J, Camara Y, Shi Y, Pellegrini M, Gaspari M, et al. MTERF3 is a negative regulator of mammalian mtDNA transcription. Cell 2007;130(2):273–85.
[54] Sailaja BS, Cohen-Carmon D, Zimmerman G, Soreq H, Meshorer E, et al. Stress-induced epigenetic transcriptional memory of acetylcholinesterase by HDAC4. Proc Natl Acad Sci 2012;109(52):E3687–95.
[55] Vercauteren K, Pasko RA, Gleyzer N, Marino VM, Scarpulla RC, et al. PGC-1-related coactivator: immediate early expression and characterization of a CREB/NRF-1 binding domain associated with cytochrome c promoter occupancy and respiratory growth. Mol Cell Biol 2006;26(20):7409–19.
[56] Athar F, Parnaik VK. Association of lamin A/C with muscle gene-specific promoters in myoblasts. Biochem Biophys Rep 2015;4:76–82.
[57] Kaul R, Purushothaman P, Uppal T, Verma SC, et al. KSHV lytic proteins K-RTA and K8 bind to cellular and viral chromatin to modulate gene expression. PloS One 2019;14(4):e0215394.
[58] Atasoy IL, Dursun E, Gezen-Ak D, Metin-Armagan D, Ozturk M, Yilmazer S, et al. Both secreted and the cellular levels of BDNF attenuated due to tau hyperphosphorylation in primary cultures of cortical neurons. J Chem Neuroanat 2017;80:19–26.
[59] Parry WL, Hemstreet GP 3rd. Cancer detection by quantitative fluorescence image analysis. J Urol 1988;139(2):270–4.
[60] Madeira F, Park YM, Lee J, Buso N, Gur T, Madhusoodanan N, et al. The EMBL-EBI search and sequence analysis tools APIs in 2019. Nucleic Acids Res 2019;47(W1):W636–41.
[61] Mahony S, Benos PV. STAMP: a web tool for exploring DNA-binding motif similarities. Nucleic Acids Res 2007;35:W253–8 Web Server issue.
[62] Roth JA, Rosenblatt T, Lis A, Bucelli R, et al. Melatonin-induced suppression of PC12 cell growth is mediated by its Gi coupled transmembrane receptors. Brain Res 2001;919(1):139–46.
[63] Chen KS, DeLuca HF. Cloning of the human 1 alpha,25-dihydroxyvitamin D-3 24-hydroxylase gene promoter and identification of two vitamin D-responsive elements. Biochim Biophys Acta 1995;1263(1):1–9.
[64] Kephart DD, Walfish PG, DeLuca H, Butt TR, et al. Retinoid X receptor isotype identity directs human vitamin D receptor heterodimer transactivation from the 24-hydroxylase vitamin D response elements in yeast. Mol Endocrinol 1996;10(4):408–19.
[65] Cuppari A, Fernandez-Millan P, Battistini F, Tarres-Sole A, Lyonnais S, Iruela G, et al. DNA specificities modulate the binding of human transcription factor A to mitochondrial DNA control region. Nucleic Acids Res 2019;47(12):6519–37.
[66] Ashcroft SP, Bass JJ, Kazi AA, Atherton PJ, Philp A, et al. The vitamin D receptor regulates mitochondrial function in C2C12 myoblasts. Am J Physiol Cell Physiol 2020;318(3):C536–41.
[67] Hossein-nezhad A, Holick MF. Vitamin D for health: a global perspective. Mayo Clin Proc 2013;88(7):720–55.
[68] Pickrell AM, Youle RJ. The roles of PINK1, parkin, and mitochondrial fidelity in Parkinson's disease. Neuron 2015;85(2):257–73.
[69] Gomez-Sanchez R, Yakhine-Diop SM, Bravo-San Pedro JM, Pizarro-Estrella E, Rodriguez-Arribas M, Climent V, et al. PINK1 deficiency enhances autophagy and mitophagy induction. Mol Cell Oncol 2016;3(2):e1046579.
[70] Helzer KT, Hooper C, Miyamoto S, Alarid ET, et al. Ubiquitylation of nuclear receptors: new linkages and therapeutic implications. J Mol Endocrinol 2015;54(3):R151–67.
[71] Rybchyn MS, De Silva WGM, Sequeira VB, McCarthy BY, Dilley AV, Dixon KM, et al. Enhanced repair of UV-induced DNA damage by 1,25-dihydroxyvitamin D(3) in skin is linked to pathways that control cellular energy. J Invest Dermatol 2018;138(5):1146–56.
[72] Slominski AT, Kim TK, Slominski RM, Song Y, Janjetovic Z, Podgorska E, et al. Metabolic activation of tachysterol(3) to biologically active hydroxyderivatives that act on VDR, AhR, LXRs, and PPARgamma receptors. FASEB J 2022;36(8):e22451.
[73] Slominski AT, Kim TK, Janjetovic Z, Brozyna AA, Zmijewski MA, Xu H, et al. Differential and overlapping effects of 20,23(OH)(2)D3 and 1,25(OH)(2)D3 on gene expression in human epidermal keratinocytes: identification of AhR as an alternative receptor for 20,23(OH)(2)D3. Int J Mol Sci 2018;19(10):3072. doi:10.3390/ijms19103072.
[74] Slominski AT, Kim TK, Takeda Y, Janjetovic Z, Brozyna AA, Skobowiat C, et al. RORalpha and ROR gamma are expressed in human skin and serve as receptors for endogenously produced noncalcemic 20-hydroxy- and 20,23-dihydroxyvitamin D. FASEB J 2014;28(7):2775–89.
[75] Slominski AT, Chaiprasongsuk A, Janjetovic Z, Kim TK, Stefan J, Slominski RM, et al. Photoprotective properties of vitamin D and lumisterol hydroxyderivatives. Cell Biochem Biophys 2020;78(2):165–80.
[76] Slominski AT, Kim TK, Qayyum S, Song Y, Janjetovic Z, Oak ASW, et al. Vitamin D and lumisterol derivatives can act on liver X receptors (LXRs). Sci Rep 2021;11(1):8002.
[77] Ito I, Waku T, Aoki M, Abe R, Nagai Y, Watanabe T, et al. A nonclassical vitamin D receptor pathway suppresses renal fibrosis. J Clin Invest 2013;123(11):4579–94.
[78] Turunen MM, Dunlop TW, Carlberg C, Vaisanen S, et al. Selective use of multiple vitamin D response elements underlies the 1 alpha,25-dihydroxyvitamin D3-mediated negative regulation of the human CYP27B1 gene. Nucleic Acids Res 2007;35(8):2734–47.

[79] Kaufman BA, Durisic N, Mativetsky JM, Costantino S, Hancock MA, Grutter P, et al. The mitochondrial transcription factor TFAM coordinates the assembly of multiple DNA molecules into nucleoid-like structures. Mol Biol Cell 2007;18(9):3225–36.
[80] Safdar A, Little JP, Stokl AJ, Hettinga BP, Akhtar M, Tarnopolsky MA, et al. Exercise increases mitochondrial PGC-1 alpha content and promotes nuclear-mitochondrial cross-talk to coordinate mitochondrial biogenesis. J Biol Chem 2018;293(13):4953.
[81] Savkur RS, Bramlett KS, Stayrook KR, Nagpal S, Burris TP, et al. Coactivation of the human vitamin D receptor by the peroxisome proliferator-activated receptor gamma coactivator-1 alpha. Mol Pharmacol 2005;68(2):511–17.
[82] Eyles DW. Vitamin D: brain and behavior. JBMR Plus 2021;5(1):e10419.
[83] Almeras L, Eyles D, Benech P, Laffite D, Villard C, Patatian A, et al. Developmental vitamin D deficiency alters brain protein expression in the adult rat: implications for neuropsychiatric disorders. Proteomics 2007;7(5):769–80.
[84] McGrath J, Iwazaki T, Eyles D, Burne T, Cui X, Ko P, et al. Protein expression in the nucleus accumbens of rats exposed to developmental vitamin D deficiency. PLoS One 2008;3(6):e2383.
[85] Keisala T, Minasyan A, Lou YR, Zou J, Kalueff AV, Pyykko I, et al. Premature aging in vitamin D receptor mutant mice. J Steroid Biochem Mol Biol 2009;115(3-5):91–7.
[86] Kauppila TES, Kauppila JHK, Larsson NG. Mammalian mitochondria and aging: an update. Cell Metab 2017;25(1):57–71.
[87] Mazzaferro S, Pasquali M. Vitamin D: a dynamic molecule. How relevant might the dynamism for a vitamin be? Nephrol Dial Transplant 2016;31(1):23–30.
[88] Herholz M, Cepeda E, Baumann L, Kukat A, Hermeling J, Maciej S, et al. KLF-1 orchestrates a xenobiotic detoxification program essential for longevity of mitochondrial mutants. Nat Commun 2019;10(1):3323.